

# Algebraic non-Hermitian skin effect and unified non-Bloch band theory in arbitrary dimensions

Kai Zhang,<sup>1</sup> Chang Shu,<sup>1</sup> and Kai Sun<sup>1,\*</sup>

<sup>1</sup>*Department of Physics, University of Michigan Ann Arbor, Ann Arbor, Michigan, 48109, United States*

(Dated: June 12, 2024)

The non-Hermitian skin effect, characterized by a proliferation of exponentially-localized edge modes in open-boundary systems, has led to the discovery of numerous novel physical phenomena that challenge the limits of conventional band theory. In sharp contrast to the traditional exponential localization, this manuscript reports a new kind of non-Hermitian skin effect, which we term the “algebraic non-Hermitian skin effect.” This effect emerges across a diverse spectrum of non-Hermitian systems in both two- and higher space dimensions. For 2D systems with algebraic non-Hermitian skin effect, on geometries such as a torus or cylinder, these systems exhibit behavior reminiscent of the conventional non-Hermitian skin effect, where eigenmodes are either bulk Bloch waves (on a torus) or exponentially localized edge modes (on a cylinder). However, if the same system is placed on a disk or any geometrical shape featuring open boundaries in all directions, the skin modes immediately transform into the algebraic form, with amplitude decaying as a power-law function of the distance from the boundary. This power-law decay, coupled with the sensitivity of edge mode decay to the real-space topology, cannot be characterized within the existing theoretical framework of the generalized Brillouin zone (GBZ). To explore these novel effects, we formulate a unified GBZ framework that is universally applicable to all variations of non-Hermitian skin effects across any spatial dimension, developed through the usage of a generalized transfer-matrix approach. Within this new framework, we find that in a  $d$ -dimensional non-Hermitian system, in general, the GBZ manifold’s dimensionality must fall into the range from  $d$  to  $2d - 1$ , denoted by  $d \leq \dim \text{GBZ} \leq 2d - 1$ . In 1D, this inequality is trivial because the upper and lower bounds converge, forcing the GBZ’s dimensionality to match with that of the physical space, in agreement with existing knowledge on the exponential non-Hermitian skin effect. However, in 2D and above, this inequality indicates that there is no obligation for the GBZ’s dimensionality to concur with the physical space’s dimensionality, which gives rise to a new class of non-Hermitian skin effects, specifically, the algebraic non-Hermitian skin effect. We have implemented this framework on tight-binding Hamiltonians to exemplify our findings within both two- and three-dimensional settings. This investigation not only unveils a novel category of the non-Hermitian skin effect but also offers a comprehensive theoretical structure that describes skin effects in any non-Hermitian system, irrespective of spatial dimensionality.

## I. INTRODUCTION

For systems that interact with external environments, the utilization of non-Hermitian Hamiltonians has proven effective in encapsulating core physical properties of these systems [1–3]. These non-Hermitian frameworks have been increasingly recognized for their utility in open classical-wave systems—including photonic [4–6], acoustic [7, 8], and mechanical metamaterials [9–13]—as well as in open quantum systems [14–17]. In recent years, research interest in non-Hermitian systems has surged as a result of their unique and distinct properties: non-Hermitian Hamiltonians allow complex-valued eigenvalues and relieve the requirement for eigenstates to be orthogonal to each other [18]. This deviation from the conventional norms enriched our understanding and led to the emergence of new insights and principles in physics beyond the scope of traditional band theory [19–23].

One striking phenomenon of non-Hermitian band systems is the non-Hermitian skin effect [24–47], which is characterized by the localization of almost all eigenstates at the open boundaries [48, 49], and a notable distinction between spectra under periodic and open boundary conditions [50]. This effect defies traditional band theory and compels a reevaluation of well-established principles, such as the bulk-boundary

correspondence that characterizes Hermitian systems [35–37, 51, 52]. Furthermore, the non-Hermitian skin effect spawns a variety of fascinating phenomena unique to non-Hermitian systems, including non-reciprocal responses [53–55], directional wavepacket invisibility [56–61], and improved sensitivity in sensors that scales with the size of the system [62–64], among others [65–67]. Such advancements hold promise for robust and adaptable control over wave and signal transmission [68, 69]. To fully comprehend the non-Hermitian skin effect, it is necessary to consider an extension of Bloch wavevectors into the complex plane, thereby advancing Bloch band theory into the more encompassing non-Bloch band paradigm [14, 24, 26, 31, 34–37, 70]. This evolution of the theory accounts for the emergent complexities and novel behaviors witnessed in non-Hermitian systems.

The non-Hermitian skin effect in one dimension has been well-established through the GBZ framework. By mapping the Bloch wavevector  $k$  to  $\beta = e^{ik}$ , the Brillouin zone (BZ) is mapped into a unit circle in the complex- $\beta$  plane as  $k$  varies from  $-\pi$  to  $\pi$ . To characterize the non-Hermitian skin effect, the wavevectors  $k$  are extended to complex values, and accordingly, the BZ is generalized to the GBZ, represented as piecewise analytic closed loops of  $\beta$  in the complex- $\beta$  plane [24, 26, 29, 31]. The GBZ accurately captures the localization of the skin effect, with the radius of the GBZ indicating its localization length and direction. Within this framework, the 1D non-Hermitian skin modes can be interpreted as Bloch waves modified by exponential localization prefactors. A lo-

\* sunkai@umich.edu

cal gauge transformation can be applied to transform these skin modes back to conventional Bloch waves, by removing the exponential prefactors [19, 24, 27]. This illustrates that the 1D non-Bloch band paradigm is not far from the traditional Bloch band framework, facilitated by the exponential localization law of the 1D non-Hermitian skin effect.

However, in two and higher dimensions, the exponential localization characteristic of the non-Hermitian skin effect needs reevaluation, due to the lack of an accurate high-dimensional GBZ description and the following observations. A direct extension of the 1D skin effect would be that the higher-dimensional skin effects also exhibit the same exponential localization behavior; accordingly, these skin modes should localize at the corners of open boundaries under the thermodynamic limit [71–76]. However, recent numerical and experimental observations have indicated that the skin modes universally accumulate on edges rather than corners of open-boundary geometries [77–86], representing a phenomenon without a direct 1D counterpart and lacking a unified GBZ description. Additionally, in higher dimensions, the complex open-boundary eigenenergies can cover a region of finite areas in the complex energy plane, indicating a need for a fundamentally different GBZ formulation compared to 1D systems. Given these considerations, we pose the following key questions: (i) Does the higher-dimensional skin effect inherently exhibit exponential localization? If not, what are the governing principles of its localization? (ii) Is it possible to develop a unified GBZ framework that accurately describes all forms of non-Hermitian skin effects? Although attempts have been made to adapt the GBZ formula to higher dimensions [71, 84, 87–91], achieving a unified GBZ framework that incorporates all critical aspects and precisely represents all variants of non-Hermitian skin effects continues to be a challenge and is still under debate.

In this manuscript, we report the algebraic non-Hermitian skin effect in two and higher dimensions. Under open boundary conditions (OBCs), the amplitudes of skin modes in these systems exhibit power-law decay, contrasting sharply with the exponential decay commonly seen in 1D systems. However, when the system’s geometry is modified into a cylindrical shape, the decay of the skin modes transitions to exponential. This power-law decay and the sensitivity of the decay pattern to boundary conditions are highly unconventional. In Hermitian systems, comparable behavior is only observed for very special systems under specific and fine-tuned conditions: for instance, in 2D elasticity with zero bulk modulus [92]. In these Hermitian systems, power-law and exponential edge modes arise due to a special characteristic of the underlying system—an emergent conformal symmetry which supports indefinitely many conserved quantities. Given that 2D conformal mappings are highly sensitive to the topology of the underlying geometry, they naturally give rise to exponential functions for a cylindrical geometry and power-law functions for a disk or annulus geometry [92]. Any deviation from the conformal limit eliminates this effect in these Hermitian systems. In contrast, in non-Hermitian systems, similar phenomena occur from a totally different origin, without the need for specialized conditions or fine-tuning, and there is no require-

ment for conformal symmetry to observe such phenomena. The presence of generic and robust algebraic edge modes represents a unique feature of non-Hermitian systems in 2D and above, and stands in stark contrast to what can be achieved in Hermitian setups and/or 1D non-Hermitian systems.

This finding of robust algebraic non-Hermitian skin effect is supported by establishing a unified GBZ framework that applies to any non-Hermitian system, regardless of its spatial dimensionality. The unified GBZ framework is established based on a generalized transfer-matrix approach. We demonstrate that the GBZ’s dimensionality depends on the coverage of the open-boundary continuum spectrum, and the number of GBZ constraints. In high dimensions, the GBZ constraint can be fewer than the space dimensionality, meaning that standing waves can be formed in either one direction or multiple directions, without necessarily forming along all space dimensions. According to the case of the open-boundary spectrum and the number of standing-wave conditions, we find that in  $d$ -dimensional lattice systems, the dimension of GBZ manifold ranges from  $d$  to  $2d - 1$ . We have also implemented this framework on tight-binding Hamiltonians in two and three dimensions, successfully demonstrating these new phenomena. The outcomes are in complete accord with numerical simulations, exhibiting consistency both quantitatively and qualitatively.

The remainder of the paper is organized as follows. In Sec. II, we summarize key concepts, focusing on dimensional counting to explain the emergence of algebraic skin modes in  $d > 1$  systems and their transition to exponential decay in cylindrical geometries, without delving into detailed theory analysis. In Sec. III, we introduce rigorous methodologies to derive the unified GBZ formula by employing the non-Bloch transfer matrix approach. With this exact theoretical method, we construct the GBZ, compute the open boundary spectrum/eigenstates, and prove the dimension analysis and theoretical framework outlined in Sec. II. In Sec. IV, utilizing this new GBZ formula, we prove that the reciprocal non-Hermitian skin effect is the algebraic skin effect, where the amplitudes of skin modes follow a power-law decay, instead of the conventionally expected exponential law. In Sec. V, we generalize the GBZ formulation into arbitrary  $d$  dimensions, and provide examples in three dimensions.

## II. DIMENSIONALITY ANALYSIS FOR THE GENERALIZED BRILLOUIN ZONE AND SUMMARY OF KEY CONCEPTS

Before delving into the universal GBZ formula in arbitrary spatial dimensions, we commence with an analysis of dimensionality regarding BZ and GBZ. In this section, our discussion pivots solely on qualitative aspects, leaving the meticulous formulation of the GBZ theory to be explored in the subsequent section.

Without loss of generality, here we examine a lattice system in a  $d$ -dimensional space with finite-range couplings and a finite number of degrees of freedom per unit cell ( $d \geq 1$ ). For

Hermitian systems, the dimensions of the BZ and the energy spectrum are

$$\begin{aligned}\dim \text{BZ} &= d, \\ \dim E &= 1.\end{aligned}\quad (1)$$

Here, each point in the BZ corresponds to a Bloch wave with a real wavevector  $k$ , and  $\dim E = 1$  implies that all eigenenergies of the Hamiltonian form some 1D line segments in the complex energy plane, along the real energy axis.

For non-Hermitian systems in 1D with open boundary conditions, we can substitute the BZ with the GBZ, and the aforementioned dimension counting remains

$$\begin{aligned}\dim \text{GBZ} &= d = 1, \\ \dim E &= 1.\end{aligned}\quad (2)$$

Here, each point in the GBZ represents a complex wavevector. Although eigenenergy may deviate from the real energy axis, they still form 1D line sections in the complex energy plane.

In contrast, open-boundary non-Hermitian systems with  $d > 1$  exhibit a distinct dimensional hierarchy, which is a key result from this study:

$$\begin{aligned}d \leq \dim \text{GBZ} &\leq 2d - 1, \\ \dim E &= 1 \text{ or } 2.\end{aligned}\quad (3)$$

It is crucial to underline that in spatial dimensions  $d > 1$ , the GBZ's dimension can surpass that of the spatial dimension  $d$ . This scenario is permissible exclusively in spatial dimensions beyond 1D, paving the way for higher-dimensional systems to manifest novel physical phenomena that are unattainable in 1D, such as the algebraic non-Hermitian skin effect. In addition, OBC eigenenergies could now occupy 1D lines or 2D regions on the complex plane, i.e.,  $\dim E = 1$  or 2.

In the construction of eigenstates for a given eigenenergy  $E$ , one needs to consider only a specific subset of the BZ in Hermitian setups or GBZ in non-Hermitian systems. This relevant subset will be termed the Fermi surface (FS) in the case of the BZ or the generalized Fermi surface (GFS) in connection with the GBZ. The dimensionality of the FS or GFS can be determined through the following relation:

$$\dim \text{FS} = \dim \text{BZ} - \dim E, \quad (4)$$

$$\dim \text{GFS} = \dim \text{GBZ} - \dim E. \quad (5)$$

$\dim \text{GFS}$  is a key factor in determining the characteristics of skin modes. When  $\dim \text{GFS} = 0$ , skin modes must decay exponentially with the increase in distance from the open boundaries. On the other hand, if  $\dim \text{GFS} > 0$ , the decay of edge modes may follow different functional forms, such as power-law. Using the dimension counting provided above, it becomes evident that  $\dim \text{GFS} > 0$  can only occur in dimensions greater than one,  $d > 1$ . Consequently, this implies that algebraic non-Hermitian skin effects cannot manifest in one-dimensional systems,  $d = 1$ .

## A. Hermitian systems

For a Hermitian system in  $d$  dimensions, the eigenstates of the Hamiltonian can be expressed as a superposition of Bloch waves:

$$\Psi = \sum_{\mathbf{k} \in \text{BZ}} A_{k_1, k_2, \dots, k_d} e^{i(k_1 x_1 + k_2 x_2 + \dots + k_d x_d)} \quad (6)$$

Here,  $\mathbf{k} = (k_1, \dots, k_d)$  represents the wavevector, and the collection of all possible  $\mathbf{k}$  defines a  $d$ -dimensional space, i.e., the Brillouin zone.

In the thermodynamic limit, the energy eigenvalue  $E$  becomes a function of the wavevector  $\mathbf{k}$ , leading to the dispersion relation  $E = \epsilon_n(k_1, \dots, k_d)$ , with the integer  $n$  denoting the band index. If we mark all possible energy eigenvalues on the complex energy plane, they will span a set of 1D line sections along the real axis, indicating that the energy spectrum is 1D,  $\dim E = 1$ .

For a specific eigenenergy  $E$ , the dispersion relation  $\epsilon_n(k_1, \dots, k_d) = E$  demarcates a  $(d - 1)$ -dimensional sub-space within the  $d$ -dimensional BZ, namely the equal-energy manifold. In this manuscript, we adopt the terminology from Fermi liquid theory and refer to this equal-energy manifold as the Fermi surface, which inherently possesses a dimensionality  $\dim \text{FS} = \dim \text{BZ} - \dim E = d - 1$ . As will be shown below, this concept of Fermi surface plays an important role in the construction of eigenstates of  $H$ . This is because for each given eigenenergy, the corresponding eigenstate can be written as the superposition of Bloch waves in the corresponding Fermi surface

$$\Psi_E = \sum_{\mathbf{k} \in \text{FS}} A_{k_1, k_2, \dots, k_d} e^{i(k_1 x_1 + k_2 x_2 + \dots + k_d x_d)} \quad (7)$$

where the sum over  $\mathbf{k}$  is performed over the Fermi surface for eigenenergy  $E$ .

To summarize, the dimensions of the BZ, energy spectrum, and Fermi surfaces for Hermitian systems are  $\dim \text{BZ} = d$ ,  $\dim E = 1$  and  $\dim \text{FS} = d - 1$ , respectively, as shown in Eqs. (1) and (4).

## B. 1D Non-Hermitian Systems

In this section, we briefly review the fundamental concepts and framework of 1D GBZ theory, emphasizing that 1D non-Hermitian systems maintain the same dimensional structure as their Hermitian counterparts.

Under open boundary conditions, though we can still compose eigenstates as superpositions of exponential functions, the wavevector  $k$  is no longer restricted to being real. In 1D, an OBC eigenstate may be expressed as

$$\Psi = \sum_{k \in \text{GBZ}} A_k (e^{ik})^x = \sum_{\beta \in \text{GBZ}} A_\beta \beta^x, \quad (8)$$

where  $k$  is the complex wavevector and, for the sake of simplicity, it can be represented by  $\beta = e^{ik}$ . The collection of

allowed  $k$  values forms the GBZ, extending the concept of the BZ to non-Hermitian systems with open boundaries. With  $k$  manifesting complex values, the GBZ naturally embeds within a two-dimensional space composed of  $(\text{Re } k, \text{Im } k)$ , denoting the real and imaginary parts of  $k$ , respectively.

Although embedded in a 2D momentum space, the actual dimension of GBZ is in fact less than two. This reduction results from the boundary conditions imposing extra constraints on the permitted  $\beta$  values, thereby diminishing the GBZ's dimensionality. The construction of the GBZ for 1D systems is already well-established, so we only provide a succinct example here. Consider a standard 1D tight-binding model, in which the Bloch Hamiltonian  $\mathcal{H}(k)$  is analytically continued into its non-Bloch counterpart with the substitution  $e^{ik} \rightarrow \beta$ :

$$\mathcal{H}(\beta) = t_0\beta^{-M} + t_1\beta^{-M+1} + \dots + t_{M+N}\beta^N, \quad (9)$$

where  $t_i$  denotes generally complex coefficients, with  $t_0, t_{M+N} \neq 0$ . The non-Bloch Hamiltonian  $\mathcal{H}(\beta)$  thus becomes a Laurent polynomial in the complex variable  $\beta$ . For a given complex eigenenergy  $E$ , by solving the characteristic equation  $\det[\mathcal{H}(\beta) - E] = 0$ , typically order-1 non-Bloch wave solutions  $\beta_i(E)$  will be obtained, which can be arranged by their magnitudes as  $|\beta_i(E)| \leq |\beta_{i+1}(E)|$ . Apart from the characteristic equation, boundary conditions at the two ends of the 1D chain impose another important constraint, known as the standing wave condition

$$|\beta_M(E)| = |\beta_{M+1}(E)|, \quad (10)$$

which stands as a cornerstone of 1D GBZ theory [24, 26, 29, 31, 32]. This condition ensures the formation of standing waves, which can simultaneously satisfy the OBCs at both ends, and thus allows the emergence of an extensive number of edge states, each of which is composed of two plane waves of exponential form with identical localization length, i.e., the non-Hermitian skin effect. Since the standing wave condition introduces one restriction on the values of  $\beta$ , the space encompassed by the allowable  $\beta$  values experiences a one-dimensional reduction, and thus  $\dim \text{GBZ} = 2d - 1 = 1$ .

Once the 1D GBZ is established, for each point within it (i.e., each permissible value of  $\beta$ ), the corresponding eigenenergies  $E$  can be inferred from the characteristic equation  $\det[\mathcal{H}(\beta) - E] = 0$ . As the allowable  $\beta$  values constitute a one-dimensional continuum, it follows that the admissible  $E$  values also create a one-dimensional continuum, corresponding to a set of 1D segments in the complex energy plane, that is,  $\dim E = 1$ .

For eigenstates at a specific eigenenergy,  $\Psi_E$ , not all possible complex wavevectors in the GBZ are needed. Instead, it just requires a relevant subset of the GBZ, which will be called the generalized Fermi Surface (GFS)

$$\Psi_E = \sum_{\beta \in \text{GFS}} A_\beta \beta^x. \quad (11)$$

In 1D, the dimensionality of the GFS is determined by  $\dim \text{GFS} = \dim \text{GBZ} - \dim E = 0$ . This zero dimensionality implies that the GFS consists of only a discrete set of  $\beta$ .

This set can be calculated by solving the characteristic equation while satisfying the standing wave condition in Eq. (10) simultaneously. In such cases, the wavefunction  $\Psi_E$  becomes the sum of a finite number of exponential functions in terms of  $x$ . Consequently,  $\Psi_E$  must decay exponentially at large  $x$ , if it is not a bulk Bloch wave. The fact that  $\dim \text{GFS} = 0$  in 1D is the reason why all skin modes decay exponentially in 1D non-Hermitian skin effects.

### C. Non-Hermitian Systems in $d > 1$

For  $d$ -dimensional non-Hermitian systems under open boundary conditions, we can represent eigenstates as sums of exponential functions with complex wavevectors:

$$\begin{aligned} \Psi &= \sum_{\mathbf{k} \in \text{GBZ}} A_{k_1, \dots, k_d} e^{i(k_1 x_1 + \dots + k_d x_d)} \\ &= \sum_{\beta \in \text{GBZ}} A_{\beta_1, \dots, \beta_d} \beta_1^{x_1} \beta_2^{x_2} \dots \beta_d^{x_d}, \end{aligned} \quad (12)$$

where  $\mathbf{k} = (k_1, \dots, k_d)$  and  $\beta_i = e^{ik_i}$ . Because each  $k_i$  is a complex number, the GBZ is embedded in a  $2d$ -dimensional space of  $\{\text{Re } k_1, \dots, \text{Re } k_d, \text{Im } k_1, \dots, \text{Im } k_d\}$ , or equivalently,  $\{\text{Re } \beta_1, \dots, \text{Re } \beta_d, \text{Im } \beta_1, \dots, \text{Im } \beta_d\}$ , where Re and Im represent real and imaginary parts respectively.

While the GBZ resides in a higher-dimensional space of  $2d$ , OBCs and resultant eigenvalue relations place constraints on the permissible complex wavevectors  $k_i$ . These constraints effectively confine the dimensionality of the GBZ to less than  $2d$ , captured by the following dimensional equation:

$$\dim \text{GBZ} = 2d - \text{number of GBZ constraints}, \quad (13)$$

in which ‘‘number of GBZ constraints’’ signifies the count of constraints influencing the eigenstates within the GBZ.

In analogy to 1D systems, for each spatial direction, one standing wave condition could be introduced

$$|\beta_{i, M_i}(E)| = |\beta_{i, M_i+1}(E)|, \quad (14)$$

where  $i = 1, 2, \dots, d$ . However, one principal finding of this study is that the enforcement of separate standing wave conditions for each spatial direction might not be compatible. For example, imposing simultaneous standing wave conditions for  $\beta_i$  and  $\beta_j$  ( $i \neq j$ ) can lead to contradictions, rendering it impossible to form eigenstates. Generally, the number of possible standing wave conditions one can enforce is constrained between 1 and  $d$ :

$$1 \leq \text{number of GBZ constraints} \leq d. \quad (15)$$

The lower limit, number of GBZ constraints = 1, indicates that standing wave conditions for any two distinct spatial directions are not reconcilable, thereby allowing for just one such condition for a single spatial direction. The upper limit, number of GBZ constraints =  $d$ , suggests that standing wave conditions for all distinct directions are congruent, permitting their simultaneous enforcement. Drawing from Eq. (13), at the lower limit of standing wave conditions (number of GBZ constraints = 1), the



GBZ dimension reaches  $2d - 1$ , while at the upper limit (number of GBZ constraints =  $d$ ), the GBZ dimension is reduced to  $d$ . Typically, a non-Hermitian system will fall between these extremes, hence the dimension of the GBZ lies between  $d$  and  $2d - 1$ :

$$d \leq \dim \text{GBZ} \leq 2d - 1. \quad (16)$$

This insight is a crucial outcome of our study, suggesting that a comprehensive characterization of the non-Hermitian skin effect in higher dimensions might necessitate a GBZ with a dimension exceeding that of the real-space lattice.

Regarding the OBC eigenenergies, non-Hermitian systems admit complex energy eigenvalues. Plotting all permissible energy eigenvalues on the complex energy plane, two scenarios may emerge. In the most generic scenario, these OBC eigenenergies will occupy certain 2D areas of the complex energy plane, i.e., the energy spectrum is two-dimensional ( $\dim E = 2$ ). This represents a marked departure from Hermitian systems or 1D non-Hermitian systems, where  $\dim E = 1$ . In an alternative scenario, which may arise from symmetry, fine-tuning, or other factors, the allowed OBC energy values fail to span any 2D regions on the complex energy plane. Instead, they are confined to 1D curves, and hence  $\dim E = 1$ .

For a given complex eigenenergy  $E$ , the allowed  $\beta$  values constitute a subspace within the GBZ, i.e., the generalized Fermi surface for  $E$ . Correspondingly, the eigenstate associated with this complex energy can be delineated as

$$\Psi_E = \sum_{\beta \in \text{GFS}} A_{\beta_1, \dots, \beta_d} \beta_1^{x_1} \beta_2^{x_2} \dots \beta_d^{x_d}, \quad (17)$$

where the summation of  $\beta$  extends over all possible values within the generalized Fermi surface of  $E$ . The dimension of the generalized Fermi surface is determined by the relation  $\dim \text{GFS} = \dim \text{GBZ} - \dim E$ . Therefore, the dimension of the generalized Fermi surface may vary from 0 up to  $2d - 2$ . Unlike 1D non-Hermitian systems, which are characterized by a 0-dimensional generalized Fermi surface, systems with  $d > 1$  may exhibit  $\dim \text{GFS} > 0$ . The presence of a nonzero  $\dim \text{GFS}$  indicates that the summation in Eq. (17) becomes an integration under the thermodynamic limit with OBCs. Because integrals of exponential functions can engender nearly any function form (for instance, through the Laplace transform), even though the eigenstate is built from exponential functions of the coordinates  $(x_1, \dots, x_d)$  [Eq. (17)], it can manifest extremely diverse behaviors in non-Hermitian systems where  $d > 1$ . For example, the eigenstate may turn into a power-law function of the coordinates, as demonstrated in Sec. IV. It is this richness that underpins the potential for the algebraic skin effect exclusive to non-Hermitian systems in dimensions higher than one.

Here we emphasize that in an open-boundary system with  $\dim \text{GFS} > 0$ , power-law decaying skin modes are allowed by Eq. (17). However, if we modify the geometry of the same system to a cylinder, imposing OBCs along the  $x_1$  direction and PBCs along  $x_2, x_3, \dots, x_d$ , the skin modes will become exponential. The underlying reason for this behavior is that within the cylindrical configuration, the wave vectors

$k_2, k_3, \dots, k_d$  are real and conserved due to PBCs in the corresponding directions. This effectively reduces the problem to a series of 1D systems, each characterized by a specific set of  $k_2, k_3, \dots, k_d$ . In such reduced dimensions, the skin modes are constrained to exhibit exponential decay. This phenomenon is a key characteristic of the algebraic skin effect: the decay characteristics of the skin modes are profoundly influenced by the topology of the system's underlying manifold.

#### D. Strategy to formulate the universal GBZ formula

Here, we succinctly outline our approach for deriving the GBZ formula for non-Hermitian systems in arbitrary dimensions, with comprehensive formalism to be detailed in the subsequent sections.

Consider a system of dimension  $d$ , with the system size  $L_1 \times L_2 \times \dots \times L_d$ . We can label the unit cells using integer coordinates  $(x_1, x_2, \dots, x_d)$  with  $1 \leq x_i \leq L_i$ . The transfer matrix method is employed to construct the eigenstates of the system — an exact analytic technique that systematically yields all eigenenergies and eigenstates for a given Hamiltonian [93–96]. This method has been widely used for Hermitian systems under both open and periodic boundary conditions, and it is equally effective for non-Hermitian systems.

In the transfer matrix approach, we first select an arbitrary direction in real space, say the  $x_d$  direction, and transform the bulk eigenequation of the Hamiltonian into a recursion for the coordinate  $x_d$ ,

$$\psi(x_1, \dots, x_d) = \mathbb{T}_d \psi(x_1, \dots, x_d - 1) \quad (18)$$

where  $\psi$  denotes the eigenstate of the Hamiltonian with eigenenergy  $E$ . The operator  $\mathbb{T}_d$  connects the  $\psi$  values at  $x_d$  and  $x_d - 1$ . This operator, known as the transfer matrix, is determined solely by the bulk Hamiltonian and the eigenenergy  $E$ , regardless of boundary conditions. The eigenvalues of the transfer matrix  $\mathbb{T}_d$  yield complex wavevectors  $\beta_d$ , as outlined in Eq. (17).

Using this transfer matrix, we can thereby express the eigenstate as

$$\psi(x_1, \dots, x_{d-1}, x_d) = \mathbb{T}_d^{x_d-1} \psi(x_1, \dots, x_{d-1}, 1). \quad (19)$$

Here the bulk Hamiltonian is encoded in  $\mathbb{T}$ . For a fixed  $\beta_d$ , the reduced subsystem can be treated as a  $(d-1)$ -dimensional system,  $\psi_{\beta_d}(x_1, \dots, x_{d-1})$ , and thus we can solve this  $(d-1)$ -dimensional problem using the transfer matrix method once again, defining a transfer matrix for  $x_{d-1}$ :

$$\psi_{\beta_d}(x_1, \dots, x_{d-2}, x_{d-1}) = \mathbb{T}_{d-1}^{x_{d-1}-1} \psi_{\beta_d}(x_1, \dots, x_{d-2}, 1). \quad (20)$$

Iterating this process ultimately simplifies the issue to a one-dimensional setup along the direction of  $x_1$ ,  $\psi_{\beta_d \beta_{d-1} \dots \beta_2}(x_1)$ . In this way, the  $d$ -dimensional system is reduced into a 1D system of  $\psi_{\beta_d \beta_{d-1} \dots \beta_2}(x_1)$ , supplemented by transfer matrices for the other  $d - 1$  directions which only rely on bulk properties. We can then treat this 1D problem as a 1D non-Hermitian system, where the GBZ theory is well understood:

the non-Hermitian skin effect necessitates a standing wave condition for the direction of  $x_1$ . This condition ensures that standing waves can be formed to obey boundary conditions at  $x_1 = 1$  and  $x_1 = L_1$ , allowing extensive number of skin modes. However, once this condition is enforced along  $x_1$ , imposing additional standing-wave constraints in other directions is generally untenable, which will be discussed below. Thus, for other directions, we must allow all possible eigenvalues of the transfer matrices  $\mathbb{T}_2, \dots, \mathbb{T}_d$  without further stipulations.

Since the standing wave condition can typically be imposed in just one spatial direction, as previously discussed, the GBZ's complex wavevector space  $(\beta_1, \dots, \beta_d)$  characteristically spans a space of dimension  $2d - 1$ , surpassing real space dimensions  $d$  if  $d > 1$ . This distinctive characteristic underpins why non-Hermitian systems with dimensions greater than 1D can exhibit unprecedented phenomena.

As we conclude this section, it is important to draw attention to two key points. The first point is regarding the application of the standing wave condition, which can be imposed in an arbitrary direction. This flexibility implies that, depending on the choice of standing-wave-condition directions,  $d$  distinct GBZs can be defined, and each GBZ corresponds to a unique set of basis functions. Because standing wave conditions in different directions in general produces different basis functions, they are typically not compatible with each other and thus cannot be simultaneously enforced. However, it is essential to recognize that while different bases associated with different GBZs can be used, the resulting eigenvalue spectrum and eigenstates—constructed as superpositions of

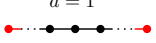

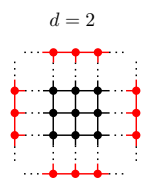

lattice	$\sigma_{\text{OBC}}$	dim GBZ	dim GFS	OBC eigenstates
$d = 1$ 	arc 	1	0	exponential skin modes or bulk waves
$d = 2$ 	area 	2	0	
		3	1	power-law, exponential skin modes, or bulk waves

FIG. 1. Dimension analysis for GBZ and GFS in 1D and 2D systems. The GBZ dimension in  $d$ -dimensional systems ranges from  $d$  to  $2d - 1$ . In 1D systems,  $\text{dim GBZ} = 1$ , and the OBC spectrum (denoted by  $\sigma_{\text{OBC}}$ ) is limited to forming arcs, meaning  $\text{dim } \sigma_{\text{OBC}} = 1$ . This leads to  $\text{dim GFS} = 0$  based on Eq. (5), with OBC eigenstates either being bulk or exponentially localized wavefunctions. In 2D systems,  $\text{dim GBZ}$  can be 2 or 3, corresponding to the standing wave conditions that are enforced in two or one spatial dimensions, respectively. The OBC spectrum in 2D generally spans a finite area in the complex energy plane,  $\text{dim } \sigma_{\text{OBC}} = 2$ . Consequently,  $\text{dim GBZ} = 0$  or 1. When  $\text{dim GFS} = 0$ , the OBC eigenstates behave as bulk or exponentially localized wavefunctions. When  $\text{dim GFS} > 0$ , the OBC eigenstates can exhibit power-law decaying behavior, a phenomenon unique to high dimensions.

these basis functions—remain invariant with respect to the choice of GBZ. Put simply, although multiple GBZ bases can be defined, they all ultimately describe the same physical reality. Secondly, although typically only one direction can accommodate the standing wave condition, special scenarios may allow the standing-wave conditions across multiple spatial directions, e.g., decoupled 1D chains populating a  $d$ -dimensional space. In such systems, GBZ dimension is further reduced to below  $2d - 1$ . If standing wave conditions for all directions are compatible with each other, the dimension of the GBZ reaches its minimum possible value, which coincides with the real-space dimensions  $d$ . This framework for 1D and 2D systems is encapsulated in Fig. 1.

### III. NON-BLOCH BAND THEORY IN TWO DIMENSIONS BASED ON THE LAYER TRANSFER MATRIX METHOD

In this section, we offer a general recipe for deriving the universal GBZ formula of 2D lattice systems using a layer transfer matrix approach. The extension of the GBZ formula to higher dimensions ( $d > 2$ ) is detailed in Section V.

To construct OBC eigenstates, we begin with the layer transfer matrix for a given tight-binding Hamiltonian. The eigenvalues of the transfer matrix dictate the propagation of the wavefunction's layer components along the transfer matrix direction. We demonstrate that a generic 2D OBC eigenstate can be represented by a superposition of standing wave components along one spatial direction (e.g., the  $x$  direction), each coupled with the corresponding allowable complex momentum  $\beta_y$  in the  $y$  direction. It is expressed as:  $\psi(x, y) = \sum_i A_i \rho_{y,i}^y \phi_i(x)$ , where  $\phi_i(x)$  represents  $i$ -th standing wave along the  $x$  direction and  $\rho_{y,i}$  is the transfer matrix eigenvalue associated with  $\phi_i(x)$ . A typical standing-wave component of an OBC eigenstate is illustrated in Fig. 2, where two equal-amplitude and counter-propagating complex waves  $\beta_{x,i}$  and  $\tilde{\beta}_{x,i}$  form standing wave  $\phi_i(x)$  in the  $x$  direction and transfer along the  $y$  direction characterized by  $\rho_{y,i}$ .

From this construction recipe for OBC eigenstates, the formation of standing waves in either one or multiple directions necessitates the corresponding GBZ conditions [Eq. (14)]. We can obtain the GBZ manifold according to the GBZ conditions. As a verification of our GBZ formula, we construct the OBC wavefunctions from the GBZ basis, which perfectly agrees with the numerical simulations.

Since the layer transfer matrix depends on the choice of layer basis, for a generic 2D Hamiltonian, the GBZ condition (or standing-wave condition) and the resultant GBZ manifold are not unique. This is fundamentally distinct from the 1D cases. However, it is worth noting that the distinct GBZ manifold only implies a basis gauge redundancy: although the GBZ manifold is not unique and depends on the layer basis, the same physical consequences and quantities will ultimately be derived.

We will detail the above main findings and conclusions in this section organized as follows: Subsections III A- III C focus on the GBZ formalism for the most generic cases in 2D,

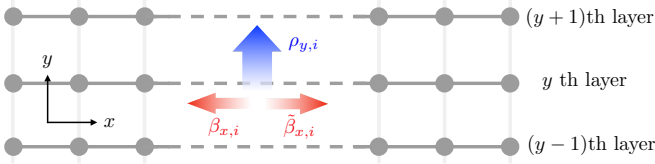


FIG. 2. Schematic of  $i$ -th standing-wave component of an OBC eigenstate under the layer- $y$  transfer matrix basis. Here, the  $i$ -th component is a standing wave  $\phi_i(x)$  in the  $x$  direction, formed by two equal amplitude and counter-propagating non-Bloch waves  $\beta_{x,i}$  and  $\bar{\beta}_{x,i}$ , coupled with the associated  $\rho_{y,i}$  in the  $y$  direction.

where  $\dim \sigma_{\text{OBC}} = 2$  and  $\dim \text{GBZ} = 3$ , as illustrated in Fig. 1. We then remark on the non-uniqueness of higher dimensional GBZ manifold and GBZ conditions in subsection III D. Finally, we discuss the GBZ formula for other 2D scenarios in subsection III E.

### A. Bulk: the non-Bloch layer transfer matrix

We start with a concrete 2D tight-binding model to present our key findings. Importantly, this methodology is universal and applicable to generic 2D systems. The model Hamiltonian in real space is given by

$$H = \sum_{x,y} t_x (c_{x+1,y}^\dagger c_{x,y} + \text{h.c.}) + t_y (c_{x,y+1}^\dagger c_{x,y} + \text{h.c.}) + t_{xy} (c_{x+1,y+1}^\dagger c_{x,y} + \text{h.c.}) + u c_{x,y}^\dagger c_{x,y}, \quad (21)$$

where  $c_{x,y}^\dagger$  denotes the creation operator of a particle at lattice site  $(x, y)$ . The Hamiltonian parameters  $t_x, t_y, t_{xy}$  indicate the hopping strengths along the  $x, y$ , and  $x+y$  directions, respectively, and  $u$  is the on-site potential. These Hamiltonian parameters are generally complex values and thus the Hamiltonian is non-Hermitian and reciprocal. This non-Hermitian Hamiltonian can be implemented in dissipative, reciprocal metamaterials [80, 81] and quantum systems [86]. Here, we utilize this reciprocal tight-binding model to demonstrate the effectiveness of our GBZ formula, which addresses the challenges in developing GBZ formulas for reciprocal non-Hermitian systems. We emphasize that our method is applicable to various systems, including non-reciprocal non-Hermitian systems. The lattice size is assumed to be  $L_x \times L_y$ . Within the layer- $y$  basis (Fig. 2), the Hamiltonian can be rewritten as

$$H = \sum_y \sum_{l=0,\pm 1} \mathbf{c}_y^\dagger \mathbf{h}_l \mathbf{c}_{y+l}, \quad (22)$$

where  $\mathbf{c}_y^\dagger$  is a row vector of creation operators at the  $y$ -th lattice layer, with  $L_x$  components, expressed as  $\mathbf{c}_y^\dagger = (c_{x=1,y}^\dagger, \dots, c_{x=L_x,y}^\dagger)$ . Under this layer basis, the Hamiltonian  $H$  can be viewed as a band Toeplitz matrix [97] of dimension  $L_y$  with matrices  $\mathbf{h}_{l=0,\pm 1}$  as its entries. The matrix

elements  $\mathbf{h}_{l=0,\pm 1}$  themselves are matrices of dimension  $L_x$  and they represent the couplings between different  $y$  layers separated by distance  $l$ . In total, the Hamiltonian is represented as a matrix of dimension  $L_y \times L_x$ . The eigenequation of the Hamiltonian is  $H\Psi_E = E\Psi_E$ , and  $\Psi_E$  is the eigenstate of eigenenergy  $E$ , represented under the layer basis as  $\Psi_E = (\psi_{y=1}, \dots, \psi_{y=L_y})^T$ . We can cast the bulk eigenequation into a recursion equation along the  $y$  direction

$$\mathbf{h}_{-1} \psi_{y-1} + (\mathbf{h}_0 - E \mathbb{I}_{L_x}) \psi_y + \mathbf{h}_1 \psi_{y+1} = 0, \quad (23)$$

where  $\mathbb{I}_{L_x}$  denotes an identity matrix of dimension  $L_x$  and  $\psi_y$  is a column with  $L_x$  components. Here,  $\psi_y$  can be further represented as  $\psi_y = (\Psi_{x=1,y}, \dots, \Psi_{x=L_x,y})^T$ , where  $\Psi_{x,y}$  indicates the wavefunction component at lattice site  $(x, y)$ . The recursion equation can be rewritten in a matrix form

$$\begin{pmatrix} \psi_{y+1} \\ \psi_y \end{pmatrix} = \mathbb{T}(E) \begin{pmatrix} \psi_y \\ \psi_{y-1} \end{pmatrix} \quad (24) \\ = \begin{pmatrix} \mathbf{h}_1^{-1}(E \mathbb{I}_{L_x} - \mathbf{h}_0) & -\mathbf{h}_1^{-1} \mathbf{h}_{-1} \\ \mathbb{I}_{L_x} & 0 \end{pmatrix} \begin{pmatrix} \psi_y \\ \psi_{y-1} \end{pmatrix},$$

where  $\mathbf{h}_1^{-1}$  is the inverse of matrix  $\mathbf{h}_1$ . This  $2L_x$ -dimensional square matrix  $\mathbb{T}(E)$ , termed the layer- $y$  transfer matrix, determines the propagation of the wavefunction's layer components along the  $y$  direction.

The transfer matrix usually takes the form of  $\mathbb{T}(k_x, E)$  when periodic boundary condition (PBC) in  $x$  direction is applied. Here, we adopt the OBCs for both the  $x$  and  $y$  directions. It is natural to extend the transfer matrix into a non-Bloch form by substituting  $e^{ik_x}$  with complex variable  $\beta_x$ . As such, the matrix elements  $h_{0,\pm 1}(k_x)$  are extended into Laurent polynomials of  $\beta_x$ , that is,  $h_{0,\pm 1}(\beta_x)$ . As an example given by Eq. (21), its non-Bloch transfer matrix under layer- $y$  basis is obtained as

$$\mathbb{T}(\beta_x, E) = \begin{pmatrix} \frac{E - h_0(\beta_x)}{h_1(\beta_x)} & \frac{-h_{-1}(\beta_x)}{h_1(\beta_x)} \\ 1 & 0 \end{pmatrix}, \quad (25)$$

where  $h_{\pm 1}(\beta_x) = t_y + t_{xy} \beta_x^{\pm 1}$  and  $h_0(\beta_x) = t_x(\beta_x + \beta_x^{-1}) + u$ . The eigenvalues of the transfer matrix  $\rho_y$  can be obtained by solving the bulk equation

$$f(\beta_x, \rho_y, E) = \det[\mathbb{T}(\beta_x, E) - \rho_y \mathbb{I}_2] \\ = \rho_y^2 + \rho_y \frac{h_0(\beta_x) - E}{h_1(\beta_x)} + \frac{h_{-1}(\beta_x)}{h_1(\beta_x)} = 0. \quad (26)$$

We use the symbol  $\rho$  to represent the eigenvalues of the non-Bloch transfer matrix, unless specified otherwise. It is worth noting that the bulk equation Eq. (26) provides constraints on  $\beta_x$  and  $\rho_y$ , which are fully equivalent to the constraints from the bulk characteristic equation  $\det[\mathcal{H}(\beta_x, \rho_y) - E] = 0$ . Here, we introduce the transfer matrix to better solve and understand the wavefunction, while introducing no new constraints. The non-Bloch transfer matrix  $\mathbb{T}(\beta_x, E)$  has two branches of eigenvalues  $\rho_y$  for each  $\beta_x$  and energy  $E$ . These two branches characterize the propagation of the non-Bloch wave  $\beta_x$  along the  $y$  direction. However, the constraints from

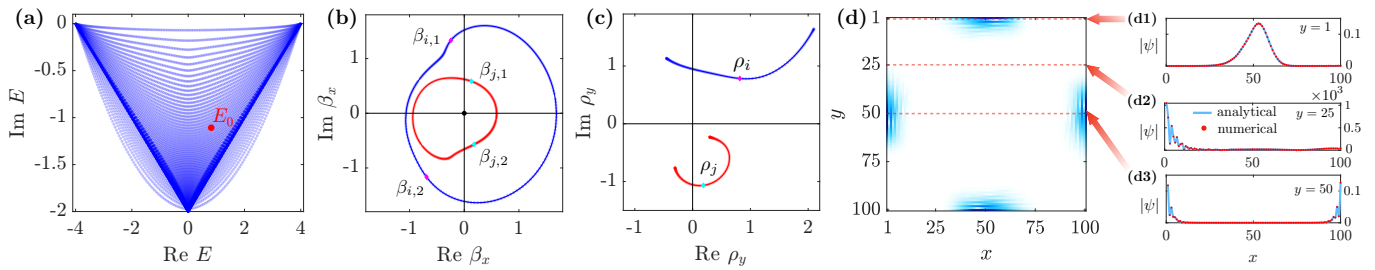


FIG. 3. The GBZ formula and the exact wavefunction constructed from GBZ basis. (a) The blue dots represent the OBC eigenvalues with the system size  $L_x=L_y=101$ . For the chosen generic energy  $E_0=0.819-1.108i$  (the red dot), the GFS projections onto the  $\beta_x$  and  $\rho_y$  planes are shown in (b) and (c), respectively. (d) The analytical wavefunction for the OBC eigenvalue  $E_0$  fully agrees with the numerical wavefunction calculated from diagonalizing the Hamiltonian matrix. The Hamiltonian parameters in Eq. (21) are set to be  $t_x = t_y = 1$ ,  $t_{xy} = i/2$ , and  $u = -i$ .

OBCs have not yet been applied at this stage. We will later demonstrate that not all  $\rho_y$  branches contribute to the open-boundary eigenstates; instead, only the branches satisfying the GBZ condition are relevant.

## B. 2D GBZ formula and standing-wave construction

Here, we focus on the GBZ formula for the most general 2D case, where  $\dim(\sigma_{\text{OBC}}) = 2$  and  $\dim(\text{GBZ}) = 3$ . According to Eq. (13), generating such a three-dimensional GBZ manifold requires a single real GBZ constraint (i.e., a standing wave condition in either one spatial direction). We present the GBZ condition and subsequently derive the GBZ manifold (or equivalently, its submanifold GFS for a specific energy). We demonstrate that in this general scenario, the 2D OBC eigenstates can be constructed using the GBZ basis, represented as a superposition of standing waves along one direction, each coupled with an associated transfer matrix eigenvalue along another direction, as illustrated in Fig. 2. Furthermore, we also discuss in subsection III E the other scenarios in two dimensions where the standing wave conditions in both two dimensions are applied and compatible with each other.

We first demonstrate that for a generic 2D lattice Hamiltonian, one can always enforce a standing wave condition along at least one spatial direction. Consider a 2D non-Bloch Hamiltonian  $\mathcal{H}(\beta_x, \beta_y)$ . Without loss of generality, fixing  $\beta_y$  reduces the 2D Hamiltonian to a 1D subsystem characterized by this fixed  $\beta_y$ . For a given energy  $E$ , generally, there exist multiple  $\beta_x$  solutions to the characteristic equation  $f(\beta_x, \beta_y, E) = 0$ . These solutions can be organized by their amplitudes as  $|\beta_{x,1}(\beta_y, E)| \leq \dots \leq |\beta_{x,M_x+N_x}(\beta_y, E)|$ , where  $M_x$  and  $N_x$  denote the maximum leftward and rightward hopping ranges, respectively, in the 1D subsystem with fixed  $\beta_y$ . For example, in the model given by Eq. (21), both  $M_x$  and  $N_x$  equal 1, indicating that the model only incorporates nearest-neighbor hopping along the  $x$  direction for a fixed  $\beta_y$ . The implementation of open-boundary conditions for the 2D system implies that OBCs also apply to each 1D subsystem with a fixed  $\beta_y$ . To reproduce the continuum spectrum for each 1D subsystem under OBCs, the following

GBZ condition inherited from the 1D non-Bloch theorem is required:

$$|\beta_{x,M_x}(\beta_y, E)| = |\beta_{x,M_x+1}(\beta_y, E)|, \quad (27)$$

which imposes a real constraint on  $(\beta_x, \beta_y, E)$ . Therefore, at least one standing-wave condition can be imposed in the most generic systems. According to Eq. (13),  $\dim \text{GBZ} = 3$  in this most generic 2D cases.

From the perspective of wavefunctions, in a generic 2D system, the OBC eigenstate can be represented as a superposition of wave components of order- $L$  ( $\mathcal{O}(L)$ ), where  $L$  stands for the system length. This is formally expressed as  $\Psi_E(x, y) = \sum_{(\beta_x, \beta_y)} A_{\beta_x \beta_y} \beta_x^x \beta_y^y$ . These order- $L$  wave components are typically required to satisfy the order- $L$  degrees of freedom imposed by the open-boundary conditions. It means that, when the system size tends to infinity (in the continuum limit), the solution domain of  $(\beta_x, \beta_y)$  should be a 1D submanifold embedded in  $\mathbb{C}^2$ . In Hermitian systems, this 1D manifold is the Fermi surface that provides the suitable Bloch wave basis for forming the open-boundary standing waves. However, in 2D non-Hermitian systems, for a fixed energy  $E$ , with only the constraints from the characteristic equation,  $\text{Re } f(\beta_x, \beta_y, E) = \text{Im } f(\beta_x, \beta_y, E) = 0$ , the solution domain of  $(\beta_x, \beta_y)$  is confined to a 2D surface within the 4D space spanned by  $\{\text{Re } \beta_x, \text{Im } \beta_x, \text{Re } \beta_y, \text{Im } \beta_y\}$ . Therefore, an additional constraint—the GBZ condition—is necessary to further reduce this domain to 1D curves, called GFS curves, which enables the proper construction of OBC eigenstates using the non-Bloch basis  $(\beta_x, \beta_y)$  on the GFS. This GBZ condition is exactly the standing wave condition along either one spatial direction, e.g., the standing wave condition enforced in the  $x$  direction as given by Eq. (27). For general 2D systems, we have  $\dim \text{GFS} = 1$ , and the OBC spectrum consistently occupies a finite region, i.e.,  $\dim \sigma_{\text{OBC}} = 2$ . Based on the relationship in Eq. (5),  $\dim \text{GBZ} = 3$  in this most generic 2D cases. Therefore, we can only enforce one standing wave condition along a single spatial direction. The imposition of an additional standing wave condition would decrease the GBZ dimension to 2 and the GFS dimension to 0, which leads to contradictions. To summarize, in the most generic 2D scenarios, it is permissible and required to enforce just one standing



wave condition along either one space dimension. The requirement for two simultaneous standing wave enforcement necessitates more precise adjustments, which we address in subsection III E.

For a given energy  $E_0$ , the GBZ condition, together with the characteristic equation in Eq. (26), determines the 1D GFS curves in the complex momenta space spanned by  $(\beta_x, \beta_y)$ . As  $E_0$  sweeps through the entire 2D OBC spectrum, the corresponding GFS constitutes a 3D GBZ manifold. From the GBZ condition in Eq. (27), we see that for a given  $\beta_y$ , the corresponding  $\beta_x$  solutions can form the standing wave along the  $x$  direction.

The GBZ condition in Eq. (27) implies the following general recipe for constructing the OBC eigenstate for a given energy  $E$ : First, let the non-Bloch wave components  $\beta_x$  to form standing waves that are satisfying the open boundary conditions in the  $x$  direction; then transfer these standing waves along the  $y$  direction through the non-Bloch transfer matrix in Eq. (25) and the GBZ condition in Eq. (27). Therefore, each standing wave in the  $x$  direction is coupled with the corresponding transfer matrix eigenvalue  $\rho_y$ . Finally, let these standing-wave components superimpose to meet the open boundary conditions in the  $y$  direction; the superposition coefficients can be determined and exact open-boundary wavefunction is eventually obtained. Based on this construction recipe, the wavefunction of energy  $E$  can be expressed as

$$\Psi_E(x, y) = \sum_{\rho_y \in \text{GFS}} A(\rho_y) \rho_y^y \phi_{\rho_y}(x), \quad (28)$$

where  $\phi_{\rho_y}(x)$  represents the standing-wave component in the  $x$  direction and  $A(\rho_y)$  represents the superposition coefficient. The standing wave component can be further expressed as:

$$\phi_{\rho_y}(x) = \sum_{j=1}^{M_x+N_x} B_j(\rho_y) \beta_{x,j}^x(\rho_y, E), \quad (29)$$

where  $B_j(\rho_y)$  represents the superposition coefficients that should satisfy the OBCs in the  $x$  direction, and  $\beta_{x,j}^x(\rho_y, E)$  satisfies the GBZ condition given in Eq. (27).

We take the Hamiltonian in Eq. (21) as an example, where the Hamiltonian only involves the nearest-neighbor hopping along the  $x$  direction, thus  $M_x = N_x = 1$ . In this model, the GBZ condition under layer- $y$  basis becomes

$$|\beta_{x,1}(\rho_y, E)| = |\beta_{x,2}(\rho_y, E)|. \quad (30)$$

The open-boundary eigenvalues with system size  $L_x = L_y = 101$  are represented by the blue dots in Fig. 3(a), which covers a finite region in the complex energy plane, i.e.,  $\dim \sigma_{\text{OBC}} = 2$ . We take a generic OBC eigenvalue  $E_0 = 0.819 - 1.108i$ , as labeled by the red dot in Fig. 3(a). The corresponding GFS can be obtained according to the GBZ condition in Eq. (30). The projection of GFS onto complex  $\beta_x$  and  $\rho_y$  planes are illustrated in Figs. 3(b) and (c), respectively. In our calculation,  $2L_x$  values of  $\rho_y$  are obtained as the eigenvalues of the layer- $y$  transfer matrix  $\mathbb{T}(E)$  given in Eq. (24). Consequently, these  $2L_x$  solutions of  $\rho_y$ , represented by blue and red dots in Fig. 3(c), form two arcs in the complex  $\rho_y$  plane. Here, we

emphasize that the 1D GFS curves in the continuum limit can be analytically obtained, similar to solving for the GBZ curves and OBC continuum bands in 1D systems [31]. Specifically, the  $\beta_x$  and  $\rho_y$  projection curves [Figs. 3(b) and (c)] of the GFS in a 2D system can be viewed respectively as the GBZ curve and OBC continuum bands of a 1D system [24, 26, 29, 31]. For a given  $\rho_y = \rho_i$  there are two corresponding  $\beta_x$  solutions having the same amplitude, i.e.,  $|\beta_{i,1}(\rho_i)| = |\beta_{i,2}(\rho_i)|$ , as denoted in Figs. 3(b) and (c). These two  $\beta_x$  solutions can be used to form a standing wave coupled with  $\rho_i$ . The OBC eigenstate of energy  $E_0$  can be constructed by these standing-wave components on the GFS. To summarize, for a given energy  $E_0$ , the GBZ condition gives rise to the 1D GFS curve. These non-Bloch waves on the GFS can be used to compose the eigenstate of energy  $E_0$ , as shown in Eq. (28), and the superposition coefficients are determined by the open-boundary conditions in the  $y$  direction, as will be shown in the following subsection.

### C. The exact 2D open-boundary wavefunction from GFS basis

Here, we show that the analytic wavefunction, constructed from the GFS according to our formula, fully agrees with the numerical wavefunction obtained from the direct diagonalization of the Hamiltonian matrix, as shown in Figs. 3(d) and (d1)-(d3), thereby validating our 2D GBZ formula.

In the model Hamiltonian given by Eq. (21), the GFS corresponding to  $E_0$  is obtained and shown in Figs. 3(b) and (c). For a given  $\rho_y$ , there exist two non-Bloch waves,  $\beta_{x,1}(\rho_y)$  and  $\beta_{x,2}(\rho_y)$ , that have the same amplitude  $|\beta_{x,1}(\rho_y)| = |\beta_{x,2}(\rho_y)|$ . These non-Bloch waves combine to form a standing wave that satisfies OBCs in the  $x$  direction, which is expressed as  $\phi_{\rho_y}(x) = \beta_{x,1}^x(\rho_y) - \beta_{x,2}^x(\rho_y)$ . An OBC wavefunction is the superposition of  $2L_x$  such standing waves, each coupled with the associated  $\rho_y$ . Therefore, for this model, the standing-wave construction in Eq. 28 can be explicitly expressed as

$$\Psi_{E_0}(\mathbf{r}) = \sum_{i=1}^{2L_x} A_i \varphi_i(x, y) = \sum_{i=1}^{2L_x} A_i \rho_i^y [\beta_{i,1}^x - \beta_{i,2}^x], \quad (31)$$

where the subscripts  $x$  and  $y$  for  $\beta$  and  $\rho$  are omitted for clarity, and  $\varphi_i(x, y)$  signifies the  $i$ -th component of the open-boundary wavefunction. The  $2L_x$  pairs of non-Bloch wave components,  $(\rho_i; \beta_{i,1}, \beta_{i,2}) |_{i=1, \dots, 2L_x}$ , constitute the GFS for  $E_0$  and are represented by the red and blue dots in Figs. 3(b) and (c). The  $2L_x$  superposition coefficients  $\{A_{i=1, \dots, 2L_x}\}$  are exactly determined by the  $2L_x$  open-boundary conditions along the  $y$  direction.

The open boundary conditions in the  $y$  direction are obtained from the recursion equation Eq. (23) when  $y = 1$  and  $y = L_y$ . Plugging in  $\psi_0 = \psi_{L_y+1} = 0$ , we get

$$\begin{aligned} (\mathbf{h}_0 - E_0 \mathbb{I}_{L_x}) \psi_1 + \mathbf{h}_1 \psi_2 &= 0; \\ \mathbf{h}_{-1} \psi_{L_y-1} + (\mathbf{h}_0 - E_0 \mathbb{I}_{L_x}) \psi_{L_y} &= 0. \end{aligned} \quad (32)$$

Here, the layer wavefunction is expressed as  $\psi_y = \{\Psi_{E_0}(x=1, y), \dots, \Psi_{E_0}(x=L_x, y)\}^T$ , with each component

$\Psi_{E_0}(x, y)$  given by Eq. (31). Therefore, these two boundary equations in Eq. (32) encompass  $2L_x$  constraints on the wavefunction components. These constraints can be conveniently expressed in matrix form as follows:

$$\mathcal{M}_B(E_0) \mathbf{A} = 0, \quad (33)$$

where  $\mathbf{A}$  is a column vector of superposition coefficients  $\{A_1, \dots, A_i, \dots, A_{2L_x}\}$ , and  $\mathcal{M}_B$  is a  $2L_x \times 2L_x$  boundary matrix.

Here, the boundary matrix provides a criterion that the determinant of the boundary matrix vanishes,

$$\det[\mathcal{M}_B(E_0)] = 0, \quad (34)$$

if and only if  $E_0$  belongs to open-boundary eigenvalues. Correspondingly, the zero-energy (null) eigenvector  $\mathbf{A}$  of the boundary matrix  $\mathcal{M}_B(E_0)$  precisely determines superposition coefficients  $\{A_i\}$ . As an illustration, we calculate these superposition coefficients using the boundary matrix for energy  $E_0 = 0.819 - 1.108i$ , and obtain the constructed analytical OBC wavefunction, as shown in Fig. 3(d). As indicated by the selected three generic layers in Fig. 3(d), we compare the constructed analytical wavefunction (the blue lines) with the numerical wavefunction (the red dots) that is computed by diagonalizing the Hamiltonian matrix. The exact match confirms the validity of our established GBZ formula.

### D. The non-uniqueness of GBZ in higher dimensions

Unlike in one dimension, the GBZ (or GFS) in higher dimensions is not unique and depends on the choice of the layer basis for a given Hamiltonian. From the perspective of the wavefunction, in one dimension, the GBZ condition exactly provides the standing wave condition: non-Bloch waves that satisfy this GBZ condition can form stable standing waves under open-boundary conditions. However, in two dimensions, dimension analysis shows that a 3D GBZ manifold needs only one standing wave condition. This means that the wavefunction can only form standing waves along either one spatial dimension, instead of in both directions. Consequently, the choices of standing wave bases in different directions correspond to distinct GBZ manifolds.

For example, the Hamiltonian in Eq. (21) can also be expressed within the layer- $x$  basis. Following a similar procedure, the non-Bloch layer transfer matrix along the  $x$  direction  $\mathbb{T}(\beta_y, E)$  and the bulk equation  $f(\rho_x, \beta_y, E) = 0$  can be derived. Here,  $\rho_x$  indicates the eigenvalues of the transfer matrix along the  $x$  direction. For the example in Eq. (21), the corresponding GBZ condition under layer- $x$  basis becomes:

$$|\beta_{y,1}(\rho_x, E)| = |\beta_{y,2}(\rho_x, E)|. \quad (35)$$

Compared it with the GBZ condition given by Eq. (30) under the layer- $y$  basis, two different GBZ conditions lead to two distinct GBZs. In the layer- $x$  basis, the projection of corresponding GFS onto  $\rho_x$  plane forms arcs while the projection onto  $\beta_y$  plane forms closed curves that satisfy the GBZ condition in Eq. (35). Using this basis, the open-boundary wavefunction can be constructed by a superposition of standing

waves in the  $y$  direction, each coupled with the corresponding transfer matrix eigenvalue  $\rho_x$

$$\Psi_E(x, y) = \sum_{\rho_x \in \text{GFS}} A(\rho_x) \rho_x^x \phi_{\rho_x}(y), \quad (36)$$

where  $\phi_{\rho_x}(y)$  indicates the standing wave coupled with the transfer matrix eigenvalue  $\rho_x$ . The superimposition coefficients of these components are determined by the open-boundary conditions in the  $x$  direction. It is important to note that though the GBZ bases obtained from the layer- $x$  and layer- $y$  transfer matrix are different, the superposition coefficients are adjusted accordingly. This ensures that the same OBC wavefunction  $\Psi_E(x, y)$  and other physical quantities are ultimately produced.

### E. Discussion on other scenarios in two dimensions

Here, we discuss other 2D scenarios that require fine-tuning or occupy a parameter space of zero measure. For completeness, all 2D cases can be classified based on the coverage of the OBC spectrum and the dimensionality of GBZ. There are four potential scenarios for their combinations:  $\dim \sigma_{\text{OBC}} = 2$  or 1 and  $\dim \text{GBZ} = 3$  or 2. Previously, we demonstrated that the most generic 2D scenario features a 3D GBZ manifold and area-form OBC spectrum. Other cases, either disallowed or necessitating fine-tuning, are discussed in this section.

When the OBC eigenvalues span a finite area and  $\dim \text{GBZ} = 2$  (Fig. 1), the dimension of GFS reduces to 0, based on the relation in Eq. (5). The zero-dimensional GFS means that OBC eigenstates are formed by a discrete number of Bloch or non-Bloch waves and thus manifest as extended bulk waves or exponentially localized skin modes. This generally requires that the Hamiltonian respects certain spatial symmetry and that the open boundary geometry matches this symmetry. A representative example is as follows. For the example in Eq. (21), we set the parameters  $t_{xy} = 0$ ,  $t_x = 1$ , and  $t_y = i$ , such that the Hamiltonian is decoupled in the  $x$  and  $y$  directions

$$\mathcal{H}(\beta_x, \beta_y) = \beta_x + \beta_x^{-1} + i(\beta_y + \beta_y^{-1}). \quad (37)$$

For a specific complex energy, say  $E_0 = 1 + i$ , the  $\beta_x$  and  $\beta_y$  can be solved as four points where  $|\beta_x| = |\beta_y| = 1$ . In this case, GFS is composed of these four Bloch points, thus the GFS reduces from the 1D curves to 0D points. Correspondingly, the GBZ conditions have two constraints,  $|\beta_{x,1}(\beta_y, E)| = |\beta_{x,2}(\beta_y, E)|$  and  $|\beta_{y,1}(\beta_x, E)| = |\beta_{y,2}(\beta_x, E)|$ , and the standing waves can be enforced simultaneously along both the  $x$  and  $y$  directions. Since the GFS is 0D, when the energy scans through the entire continuum spectrum, the corresponding GBZ is a 2D manifold.

When the OBC eigenvalues form some arcs within the complex energy plane, the GBZ manifests as a 2D manifold. This implies that standing wave conditions can be enforced in both the  $x$  and  $y$  directions. We provide an intuitive argument by contradiction as follows. We begin with the assumption that  $\dim \text{GBZ} = 3$  in this arc-spectrum case. According to the relation in Eq. (5), GFS is a 2D manifold, i.e.,

$\dim \text{GFS} = 2$ . However, a 3D GBZ manifold would suggest that only one standing wave condition can be enforced based on Eq. (5). Under these conditions, once the layer- $y$  basis is selected, the OBC eigen wavefunctions are constructed based on Eq. (28). Contrasting with our initial supposition, nevertheless, the wavefunction construction here only requires order- $L$  non-Bloch solutions on the GFS, suggesting that the actual GFS consists of 1D curves, i.e.,  $\dim \text{GFS} = 1$ . Consequently, we arrive at the contradiction with the initial assumption that  $\dim \text{GBZ} = 3$  in the arc-spectrum case. Therefore, we conclude that in arc-spectrum scenarios, the GBZ manifold is 2-dimensional. One example is the 2D Hatano-Nelson model, which is given by

$$\mathcal{H}(\beta_x, \beta_y) = t_x \beta_x + w_x \beta_x^{-1} + t_y \beta_y + w_y \beta_y^{-1} \quad (38)$$

with the real valued  $t_i, w_i > 0$  and  $t_i \neq w_i$  for  $i = x, y$ . The GBZ can be directly solved through an imaginary gauge transformation:  $\beta_x \rightarrow \sqrt{w_x/t_x} \tilde{\beta}_x$ , and  $\beta_y \rightarrow \sqrt{w_y/t_y} \tilde{\beta}_y$ . After this transformation, the 2D non-Hermitian Hamiltonian is mapped to a Hermitian Hamiltonian in the basis of  $\tilde{\beta}_x$  and  $\tilde{\beta}_y$ :  $\mathcal{H}(\tilde{\beta}_x, \tilde{\beta}_y) = \sqrt{t_x w_x}(\tilde{\beta}_x + \tilde{\beta}_x^{-1}) + \sqrt{t_y w_y}(\tilde{\beta}_y + \tilde{\beta}_y^{-1})$ . For the Hermitian Hamiltonian  $\mathcal{H}(\tilde{\beta}_x, \tilde{\beta}_y)$ , the GBZ coincides with the BZ, and its GFS reduces to a  $(d-1)$ -dimensional Fermi surface. The OBC eigen wavefunctions are Bloch wave standing waves along both  $x$  and  $y$  directions. Upon transforming this Hermitian Hamiltonian back to the non-Hermitian one, we can obtain the GBZ in the original non-Hermitian Hamiltonian is a 2D distorted torus with radius  $|\beta_i| = \sqrt{w_i/t_i}$  for  $i = x, y$ . In this case, the OBC eigenstates are Bloch waves modified by an exponential prefactor, causing the wavefunctions to concentrate at the corners of open boundaries.

So far, we have exhausted all conceivable scenarios in two dimensions. It's worth noting that in these two specific fine-tuning scenarios discussed, both the GBZ and GFS can be solved through the layer transfer matrix approach. However, in these specific scenarios, the GBZ and GFS are independent of the choice of layer basis and the GBZ manifold is unique, contrasting with the non-uniqueness of GBZ for generic 2D systems. The uniqueness of the GBZ manifold here stems from the alignment of the number of standing wave conditions with the spatial dimensions. Given that these scenarios require precise fine-tuning, our primary findings in this study are focused on the more general two-dimensional systems.

#### IV. ALGEBRAIC NON-HERMITIAN SKIN EFFECT IN TWO DIMENSIONS

Through the established two-dimensional GBZ formula above, we can obtain the analytic OBC eigen wavefunctions constructed from the GBZ basis. Based on this, we demonstrate in this section that for the reciprocal non-Hermitian systems in higher dimensions, the skin modes generally follow the power-law localization. This universal algebraic skin effect is in sharp contrast to the exponential-law localization observed in conventional non-Hermitian skin effects.

Here, we prove that the reciprocal non-Hermitian systems lead to the algebraic skin effect in higher dimensions. A crucial point is that for a given energy  $E$ , when its 1D GFS curves in the complex momentum space extend through the Brillouin Zone, the resulting OBC wavefunction from the GFS basis exhibits power-law decay. In one dimension, the GFS for a given energy is 0D ( $\dim \text{GFS} = 0$ ), hence, this algebraic localization of skin effect is unique to dimensions greater than one. For demonstration, we use the model given by Eq. (21) and set the system parameters to  $t_x = 0, t_y = i, t_{xy} = 1, u = -2i$ . The non-Bloch Hamiltonian becomes

$$\mathcal{H}(\beta_x, \beta_y) = i(\beta_y + \beta_y^{-1}) + \beta_x \beta_y + (\beta_x \beta_y)^{-1} - 2i, \quad (39)$$

which respects the reciprocity,  $\mathcal{U}^\dagger H^T(\beta_x, \beta_y) \mathcal{U} = H(1/\beta_x, 1/\beta_y)$ , with the unitary matrix satisfying  $\mathcal{U} \mathcal{U}^* = 1$ .

When the Hamiltonian respects reciprocity, it exhibits the spectral property that OBC bulk eigenvalues belong to the Bloch spectrum, denoted as  $E_{\text{OBC}} \in \sigma_{\text{PBC}}$ . See a detailed proof in Appendix A. As a result, for a given OBC eigenvalue  $E_0$  in reciprocal systems, there are always Bloch wave solutions  $\mathbf{k}_i$  obtained by solving  $\det[h(k_x, k_y) - E_0] = 0$  where  $h(k_x, k_y)$  denotes the Bloch Hamiltonian. These Bloch wave solutions, termed Fermi points, are related by reciprocity. In the above example with Hamiltonian given by Eq. (39), the Bloch spectrum is represented by the blue region in Fig. 4(a), and open-boundary eigenvalues for a system size of  $L_x = L_y = 81$  are indicated by red dots in Fig. 4(a). We select a generic OBC eigenvalue  $E_0 = 0.61 - 0.58i$ , denoted by the blue dot in Fig. 4(a). The distribution of the corresponding Fermi points in the Brillouin zone is illustrated in Fig. 4(b).

As shown in Fig. 4(b), a pair of Fermi points  $\mathbf{k}_1$  and  $\mathbf{k}'_1$  (or  $\mathbf{k}_2$  and  $\mathbf{k}'_2$ ) have the same projection  $k_{y,1}$  ( $k_{y,2}$ ) on the  $k_y$  axes. We can always let Bloch waves  $k_{x,1}$  and  $k_{x,3}$  form a standing wave, which is extended along the  $x$  direction, and then transfer this standing wave along the  $y$  direction, characterized by  $k_{y,1}$ . According to our standing-wave construction in Eq. (31), the OBC wavefunction of  $E_0$  encompasses this standing-wave component:  $\phi_{k_{y,1}}(x, y) = e^{ik_{y,1}y}(e^{ik_{x,1}x} - e^{ik_{x,3}x})$ . The GFS for  $E_0$  is obtained using the transfer matrix approach under the layer- $y$  basis, and its projections onto the  $\beta_x$  and  $\rho_y$  planes are shown in Figs. 4(c) and (d), respectively. The presence of Fermi points for  $E_0$  means that its GFS must cross the Brillouin zone, as represented by the black unit circle in Figs. 4(c) and (d). These intersections, labeled by purple and green dots, correspond to the Fermi points in Fig. 4(b), specifically  $\rho_{y,i} = e^{ik_{y,i}}$  and  $\beta_{x,i} = e^{ik_{x,i}}$ . In the continuum limit, the projection of the GFS on the  $\rho_y$  plane forms 1D curves that cross the unit circle. Consequently, in reciprocal non-Hermitian systems, a generic OBC eigen wavefunction invariably encompasses Bloch standing wave components, characterized by  $|\rho_y| = |\beta_x| = 1$ . The intersections between GFS and the Brillouin zone are guaranteed by the reciprocity of the Hamiltonian. These intersection points give rise to Bloch standing wave components of the OBC wavefunction. Next, we demonstrate that the presence of these Bloch wave components in the OBC wavefunction leads to the power-law localization.

We focus on the intersection point  $\rho_{y,1}$ , which is relabeled by  $\rho_0$  for notational clarity as shown in Fig. 4(d). In the continuum limit, the summation over  $\rho_y$  points in the wavefunction of Eq. (31) becomes the integral over the  $\rho_y$  curve. The contribution of wave components near the intersection  $\rho_0$  is described by

$$\Psi_{E_0, \rho_0}(x, y) = \int_{\delta\rho} d\rho A(\rho) \rho^y [\beta_1^x(\rho) - \beta_2^x(\rho)], \quad (40)$$

where  $\delta\rho$  represents a piece of  $\rho_y$  that is a small deviation from the  $\rho_0$ . Here, we study the localization of wavefunction at the

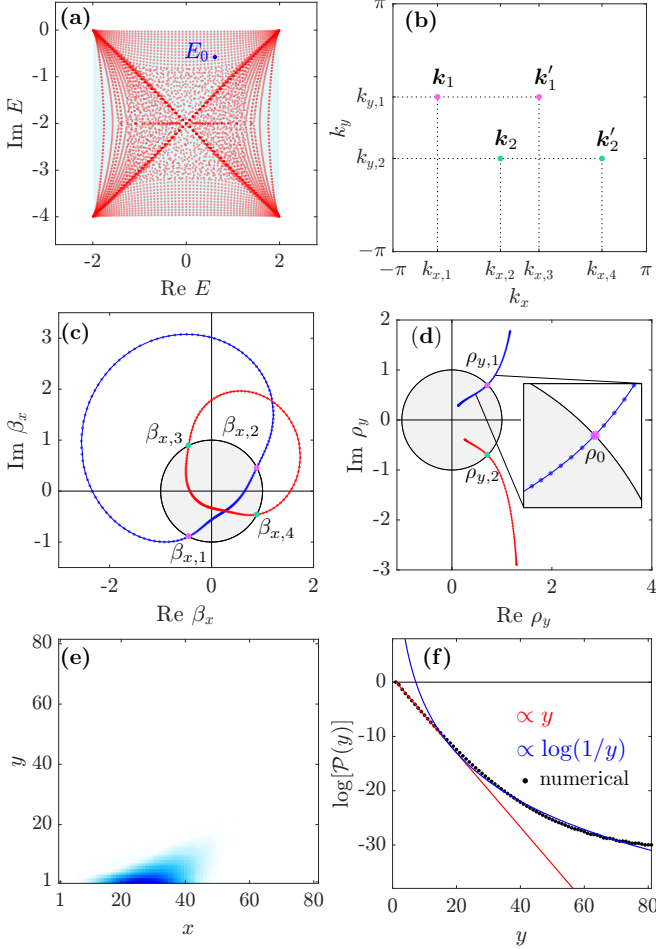


FIG. 4. The power-law localization of non-Hermitian skin effect. (a) The comparison between the PBC spectrum (the blue region) and OBC eigenvalues (the red dots), with the system size of  $L_x = L_y = 81$ . (b) For the selected OBC eigenvalue  $E_0 = 0.61 - 0.58i$  (the blue dot in (a)), there are four corresponding Fermi points  $\mathbf{k}_i$  distributed in Brillouin zone, where  $\det[h(\mathbf{k}_i) - E_0] = 0$ . The projections of the GFS of  $E_0$  on the  $\beta_x$  and  $\rho_y$  planes are shown in (c) and (d), respectively. The intersections between the GFS and the Brillouin zone (the black unit circle) are labeled by the purple and green dots, which correspond to the four Fermi points in (b). (e) The partial wavefunction that is constructed from the GFS inside the unit circle. (f) The layer density of the wavefunction exhibits power-law localization when it is away from the edge.

bottom edge of the system. Therefore, we only select the  $\rho_y$  components inside the unit circle and neglect the components outside. Hence, we choose  $|\rho_y| \leq 1$  as the integral region. According to 2D GBZ condition in Eq. (30), we have  $|\beta_1(\rho)| = |\beta_2(\rho)| = e^{\mu_x(\rho)}$ . Consequently, the standing wave component in Eq. (40) becomes  $\beta_1^x(\rho) - \beta_2^x(\rho) = e^{\mu_x(\rho)x} \sin(\theta_\rho x)$ , where  $\theta_\rho$  is the real-valued phase difference that depends on  $\rho$ . The intersection  $\rho_0$  corresponds to  $\beta_{x,1}$  and  $\beta_{x,2}$  in the  $\beta_x$  plane, where  $|\beta_{x,1}| = |\beta_{x,2}| = 1$ . Near  $\rho_0$  and within the unit circle,  $|\beta_x(\rho)| \lesssim 1$  and  $\mu_x(\rho) \lesssim 0$ . The function  $\mu_x(\rho)$  can be approximated as  $\mu_x(\rho) = \mu_x(\rho_0) + \mu'_x(\rho_0) \delta\rho + o(\delta\rho) \approx \mu_x(\rho_0) = 0$ , where only the leading term is retained. Adopting this approximation, the Eq. (40) can be represented as

$$\Psi_{E_0, \rho_0}(x, y) \approx \int_{\delta\rho} d\rho A(\rho) \rho^y \sin(\theta_\rho x). \quad (41)$$

We now define the layer density of the wavefunction to capture the decay law along the  $y$  direction, expressed as

$$\mathcal{P}_{E_0, \rho_0}(y) := \int dx |\Psi_{E_0, \rho_0}(x, y)|^2. \quad (42)$$

Substituting Eq. (41) into Eq. (42), noting that the cross terms will vanish due to  $\int dx \sin(\theta_{\rho_1} x) \sin(\theta_{\rho_2} x) = 0$  for  $\rho_1 \neq \rho_2$ , we finally obtain that  $\mathcal{P}_{E_0, \rho_0}(y) \approx \int_{\delta\rho} d|\rho| |A(\rho)|^2 |\rho|^{2y}$ . The layer density can be further expressed as

$$\mathcal{P}_{E_0, \rho_0}(y) \approx \int_{-\infty}^0 d\mu_y |A(\mu_y)|^2 e^{\mu_y(2y+1)}, \quad (43)$$

where  $e^{\mu_y} = |\rho|$ ,  $d|\rho| = e^{\mu_y} d\mu_y$ , and  $\mu_y \leq 0$  in this integral region. Here,  $|A(\mu_y)|^2$  corresponds to the superposition coefficients. It can be expanded near the  $\mu_y = 0$  as  $|A(\mu_y)|^2 = |A_0|^2 + |A_1|^2 \delta\mu_y + o(\delta\mu_y)$  with  $A_0 \equiv A(\mu_y = 0)$ . Finally, the leading order for the localization law of the layer wavefunction density becomes

$$\mathcal{P}_{E_0, \rho_0}(y) \sim |A_0|^2 y^{-1} + o(y^{-1}), \quad (44)$$

where  $|A_0|^2 \neq 0$  is ensured when the open-boundary wavefunction includes the Bloch standing wave components, which holds true when the Hamiltonian respects reciprocity. So far, we have demonstrated that the presence of Bloch standing wave components leads to the universal power-law decay of  $r^{-1}$  for the open-boundary wavefunctions, where  $r$  is the distance from the open boundaries.

The verification of power-law localization of wavefunction is shown in Figs. 4(e) and (f). To present the contribution of Bloch standing wave components more clear, we consider the partial OBC wavefunction that is constructed by the non-Bloch bases of GFS inside and on the unit circle, as denoted by the gray regions in Figs. 4(c) and (d). As shown in Fig. 4(e), this partial wavefunction is localized at the bottom edge  $y$  due to localization length  $\mu_y \leq 0$ . Due to the reciprocity, the other part of the wavefunction constructed by the non-Bloch bases outside the unit circle will be localized at the top edge  $y$  and is center-symmetric about the origin of the lattice. We calculate the layer density for this partial wavefunction, as shown by the black dots in Fig. 4(f), where the blue and red curves represent



TABLE I. Based on the number of standing wave conditions (in the horizontal direction) and the case of the open-boundary spectrum (in the vertical direction), the dimensions of GBZ and GFS in  $d$ -dimensional lattice systems are summarized in the following table.

	$n = 1$	$1 \leq n \leq d$	$n = d$	
arc spectrum ( $d = 1$ )			$d$ $d - 1$	dim GBZ dim GFS
area spectrum ( $d \geq 2$ )	$2d - 1$ $2d - 3$	$2d - n$ $2d - n - 2$	$d$ $d - 2$	dim GBZ dim GFS

the exponential- and power-law fitting, respectively. It shows that the OBC wavefunction follows a power law tail of  $y^{-1}$  when it moves away from the edge.

Remarkably, the power-law decay behavior is robust even with the finite-size system. For a system size of  $L_x \times L_y$ , there are  $2L_x$  solutions for  $\rho_y$ . As shown in the inset of Fig. 4(d), it exhibits a minor gap between  $\rho_y$  solutions and the unit circle. The gap scales with the length of  $L_x$  and can be quantified as  $\log \Delta \sim \alpha/L_x$ , where  $\alpha > 0$  is a constant factor. This gap, determined solely by the length  $L_x$  and independent of  $L_y$ , modifies the upper limit of the integral in Eq. (43) to  $-\alpha/L_x$ . Consequently, the average density with length of  $L_x$  becomes:

$$\mathcal{P}_{E_0, \rho_0, L_x}(y) \sim y^{-1} e^{-\alpha y/L_x}, \quad (45)$$

which exponentially converges to a perfect power-law decay in Eq. (44) as  $y$  increases. It concludes that the finite-size effects on decay behavior along the  $y$  direction are entirely controlled by the system length  $L_x$  in the  $x$  direction. This is derived from the fact that a finite-size wavefunction is composed of  $2L_x$  non-Bloch wave components and is independent of the length in the  $y$  direction, hence establishing that the  $L_x$ -dependence of the power-decay behavior in the  $y$  direction. This inter-dependency between the system length in the  $x$  direction and the convergence rate to power-law decay in the  $y$  direction is a characteristic feature of the algebraic non-Hermitian skin effect in a finite-size lattice system.

## V. THE GBZ FORMULA IN GENERIC HIGHER DIMENSIONAL SYSTEMS

So far, we have established the GBZ formula in two dimensions using the layer transfer matrix method and derived the algebraic non-Hermitian skin effect. We now extend these formulas to generic higher dimensions.

In two dimensions, we show that, unlike in one dimension, the number of standing wave conditions can be either one or two, producing a 3D or 2D GBZ manifold, respectively. In  $d$  dimensions, the complex momenta span a  $2d$ -dimensional real space, and the number of standing wave conditions can be within the range of  $1 \leq n \leq d$ . Correspondingly, the GBZ dimension is determined to be  $2d - n$ . Therefore, for a  $d$ -dimensional lattice system, the dimension of the GBZ mani-

fold is in the range:

$$d \leq \dim \text{GBZ} \leq 2d - 1. \quad (46)$$

The GFS is related to the GBZ through the open-boundary spectrum, and they have the dimensionality relation:  $\dim \text{GFS} = \dim \text{GBZ} - \dim E$ . Notably, when  $d = 1$ , this inequality in Eq. (46) constrains the GBZ manifold to one dimension, and the open-boundary spectrum is restricted to forming some arcs in the complex energy plane, namely  $\dim E = 1$ . Consequently, for a given OBC eigenvalue, the GFS consists of some points and has the dimensionality of  $\dim \text{GFS} = \dim \text{GBZ} - \dim E = 0$ . When  $d \geq 2$ , the case of GFS becomes more complicated due to the fact that the OBC eigenvalues can cover areas in the complex energy plane. In conclusion, the dimension of the GFS in  $d \geq 2$  dimensions falls within the range:

$$d - 2 \leq \dim \text{GFS} \leq 2d - 3, \quad \text{for } d \geq 2. \quad (47)$$

For example, in  $d = 2$ , the open-boundary spectrum covers a finite area in the complex energy plane, and the GBZ dimension could be either 2D or 3D. Correspondingly, the GFS is composed of 0D points or 1D curves. All these scenarios in two dimensions have been included in our previous discussions. The dimensions of GBZ and GFS in  $d$ -dimensional systems are concluded in Table I.

According to the dimension counting in Eq. (46) and Eq. (47), in three dimensions ( $d = 3$ ), the GBZ dimension could be 3, 4, or 5, and the GFS dimension ranges from 1 to 3. In general cases,  $\dim \text{GBZ} = 5$  and  $\dim \text{GFS} = 3$ . We now provide an example for this generic case.

For a three-dimensional non-Hermitian Hamiltonian, its open-boundary eigenvalues are typically complex-valued, and their number scales with the system size. In the most generic cases, these eigenvalues cover finite areas in the complex energy plane, that is,  $\dim E = 2$ . For this case, we can extend the transfer matrix approach to three dimensions to obtain the GBZ formula and construct the analytic open-boundary wavefunctions. To demonstrate this generalization, we consider an example of a 3D non-Bloch Hamiltonian:

$$\begin{aligned} \mathcal{H}(\beta_x, \beta_y, \beta_z) = & \sum_{i=x,y,z} t_i (\beta_i + \beta_i^{-1}) \\ & + t_{xyz} (\beta_x \beta_y \beta_z + \beta_x^{-1} \beta_y^{-1} \beta_z^{-1}), \end{aligned} \quad (48)$$

where  $t_{i=x,y,z}$  are the nearest neighbor hopping strengths along  $x, y$ , and  $z$  directions, respectively. The term  $t_{xyz} \neq 0$  represents hopping along the cube diagonal direction, effectively coupling the lower-dimensional systems in the  $x, y$ , and  $z$  directions. One can first choose the transfer matrix basis. Without loss of generality, the Hamiltonian can be written in the planar- $xy$  basis and transferred along the  $z$  direction. We assume the system size to be  $L^3$ , with  $L$  being the system length. Similar to Eq. (24), a planar transfer matrix of dimension  $2L^2 \times 2L^2$  can be obtained. The eigenvalues of this transfer matrix, denoted as  $\rho_z$ , are allowed by the bulk Hamiltonian. In general, these  $2L^2$  non-Bloch solutions of  $\rho_z$  cover a finite region in the complex  $\rho_z$  plane. For each fixed

$\rho_{z_0}$ , the 3D non-Bloch Hamiltonian Eq. (48) reduces to a 2D subsystem,  $\mathcal{H}(\beta_x, \beta_y, \rho_{z_0})$ . One can treat this 2D subsystem as a 2D system, and solve it using the layer transfer matrix approach once again in two dimensions. According to the established transfer matrix method for a 2D Hamiltonian, a 1D GFS curve in the  $(\beta_x, \rho_y)$  space can be obtained, which varies with the choice of  $\rho_{z_0}$ . For each fixed  $\rho_{z_0}$ , 1D GFS curves in the  $(\beta_x, \rho_y)$  for the 2D subsystem can be solved. As  $\rho_z$  scans through the 2D region, a 3D GFS associated with a specific energy for this 3D Hamiltonian is ultimately obtained, indicating  $\dim \text{GFS} = 3$ . Consequently, the GBZ for this Hamiltonian has the dimension  $\dim \text{GBZ} = \dim \text{GFS} + \dim E = 5$ . For each fixed  $\rho_{z_0}$  and  $\rho_{y_0}$ , the Hamiltonian reduces to 1D subsystem. Consequently, the standing wave condition along the  $x$  direction can be enforced, which gives rise to the GBZ condition for this 3D system:

$$|\beta_{x,1}(\rho_y, \rho_z, E)| = |\beta_{x,2}(\rho_y, \rho_z, E)|. \quad (49)$$

Depending on the transfer matrix basis, the GBZ condition will change and is not unique, similar to the 2D cases discussed in subsection III D. Similarly, the 3D OBC wavefunction can be constructed as follows: Let the non-Bloch waves first form standing waves along the  $x$  direction; then transfer these standing waves along the  $y$  direction to form planar components; each planar component is further transferred along the  $z$  direction to generate a standing wave component. Therefore, the OBC wavefunctions for this model can be constructed with these standing wave components:

$$\Psi_{E_0}(x, y, z) = \sum_{i=1}^{2L^2} \sum_{j=1}^{2L} A_{ij} \rho_{z,i}^z \rho_{y,j}^y (\beta_{x,1}^x - \beta_{x,2}^x), \quad (50)$$

where the tensor  $A_{ij}$  represents the superposition coefficients, and  $\beta_{x,1}$  and  $\beta_{x,2}$  depend on the values of  $\rho_{z,i}$  and  $\rho_{y,j}$  and satisfies the GBZ condition in Eq. (49). We take the Hamiltonian in Eq. (48) with the lattice size of  $L = 12$  and set the parameters to  $t_x = t_y = 1/2$ ,  $t_z = 1$ , and  $t_{xyz} = i/2$ . The analytic wavefunction, constructed from the GFS basis, fully aligns with the numerical wavefunction obtained by diagonalizing the Hamiltonian matrix. For verification details, see Appendix B. This successfully verifies the 3D generalization of the 2D GBZ formula. As an illustration, this case features a 3D GFS manifold embedded within a 5D GBZ manifold.

## VI. CONCLUSION AND DISCUSSION

In summary, this work establishes a unified GBZ formula applicable to any non-Hermitian lattice system across all spatial dimensions, developed using a non-Bloch transfer-matrix approach. We find that in  $d$ -dimensional non-Hermitian systems, the GBZ dimensionality ranges from  $d$  to  $2d - 1$ ,  $d \leq \dim \text{GBZ} \leq 2d - 1$ . Notably, in high dimensional ( $d > 1$ ) non-Hermitian systems, the GBZ dimensionality can surpass the space dimension, marking a distinct departure from both Hermitian and 1D non-Hermitian frameworks. This extended GBZ dimensionality provides a platform for new forms of

non-Hermitian skin effects in higher dimensions. Within this framework, standing wave conditions can be imposed in one or multiple spatial directions. Using the standing wave recipe, we are able to precisely construct the open-boundary wavefunctions, which aligns exactly with numerical simulations. This alignment not only provides robust evidence of the GBZ framework's correctness but also helps elucidate the fundamental characteristics of the high-dimensional skin effect. A key feature we revealed in this work is the algebraic localization in the 2D non-Hermitian skin effect, where the amplitude of skin modes follows a power-law decay with distance from open boundaries.

Contrary to conventional wisdom, which associates the non-Hermitian skin effect with exponential localization at open boundaries and insensitivity to distant local perturbations, the nature of algebraic localization indicates long-range spatial correlations in the higher-dimensional skin effect. Owing to its power-law decay, this universal algebraic skin effect cannot be fully captured by a local imaginary gauge transformation to Bloch waves, underlining its uniqueness and foundational significance in non-Hermitian higher-dimensional systems. The revelation of the long-range correlation of the high-dimensional skin effect is expected to inspire related physical consequences and provide a basis for future research.

## ACKNOWLEDGMENTS

We thank C. Fang for valuable discussions. This work was supported in part by the Office of Naval Research (MURI N00014-20-1-2479).

### Appendix A: The existence of Fermi points ensured by reciprocity

Here, we prove that the existence of Fermi points for open-boundary bulk eigenvalues is guaranteed by the reciprocity of the Hamiltonian.

For a given Bloch Hamiltonian  $h(k_x, k_y)$ , we first define the spectral winding number in the  $x$  direction with fixed  $k_y$

$$w(E_0, k_y) = \frac{1}{2\pi} \int_{-\pi}^{\pi} dk_x \partial_{k_x} \arg \det [h(k_x, k_y) - E_0], \quad (A1)$$

where  $E_0$  represents a generic OBC eigenvalue, considered as the reference energy here.

The reciprocity of the Hamiltonian ensures that the OBC bulk eigenvalues must be included in its PBC spectrum. Here, we provide a proof for this statement. Suppose an open-boundary bulk eigenvalue  $E_0 \notin \sigma_{\text{PBC}}$ , and the Hamiltonian respects reciprocity. It is known that the OBC bulk spectrum is obtained from the collapse of the PBC spectrum. Thus, the OBC bulk spectrum cannot exceed the outer boundary of the PBC spectrum. If we assume  $E_0 \notin \sigma_{\text{PBC}}$ , the only possible case is that  $E_0$  is located within an inner gap of the PBC spectrum, such as some inner holes of the PBC continuum

spectrum. Below, we prove that this case is forbidden by the reciprocity of the Hamiltonian. Consequently, open-boundary eigenvalues must belong to the PBC spectrum of  $h(k_x, k_y)$ , and for a given open-boundary eigenvalue  $E_0$ , there exist Fermi points ensured by reciprocity.

Due to the reciprocity of the Hamiltonian, the spectral winding number in Eq. (A1) satisfies  $w(E_0, k_y) = -w(E_0, -k_y)$ . At the high symmetry points  $k_y^* = 0, \pi$ , we have  $k_y^* = -k_y^*$ . Therefore, for a generic OBC eigenvalue  $E_0$ , the spectral winding number satisfies  $w(E_0, k_y^*) = -w(E_0, k_y^*) = 0$ . It means that the PBC spectrum of  $h(k_x, k_y^*)$  collapses into arcs in the complex-energy plane [29]. Similarly, the spectrum of  $h(k_x^*, k_y)$  also collapses into arcs at the high symmetry points  $k_x^* = 0, \pi$ . Assuming  $E_0$  is in the inner gap of the PBC spectrum, there is a  $k_y^0$  such that the spectrum of  $h(k_x, k_y^0)$  has a nonzero spectral winding number with respect to  $E_0$ . When we smoothly transition  $k_y$  from  $k_y^0$  to  $k_y^*$  (for example,  $k_y^* = 0$ ), the corresponding PBC spectrum of the 1D subsystem of  $k_x$  must transition smoothly. Therefore, it is impossible to squeeze the spectrum from a loop encircling energy  $E_0$  (at  $k_y = k_y^0$ ) into an arc (at  $k_y = k_y^*$ ) without passing through  $E_0$ . Consequently, the PBC spectrum must sweep through  $E_0$  at some  $k_{y,i}$ . These  $k_{y,i}$  correspond to the Fermi points of  $E_0$ . Therefore, open-boundary eigenvalue  $E_0$  must belong to the periodic-boundary spectrum of  $h(k_x, k_y)$  and the existence of Fermi points is ensured by reciprocity.

## Appendix B: The GBZ formula in three-dimensional systems

Here we provide a detailed numerical verification for GBZ formula of the 3D tight-binding model given by Eq. (48). This section includes two steps: First, we choose the proper planar basis and obtain the GFS/GBZ under this basis. In the most generic cases,  $\dim \text{GFS} = 3$  and  $\dim \text{GBZ} = 5$ . Second, for a specific OBC eigenvalue, we can construct the corresponding OBC eigen wavefunction using the GFS basis, which perfectly match the numerical wavefunction obtained by diagonalizing the Hamiltonian matrix.

The real space Hamiltonian for model given by Eq. (48) is written as

$$\begin{aligned}
 H = & \sum_{x,y,z} t_x (c_{x+1,y,z}^\dagger c_{x,y,z} + \text{h.c.}) + t_y (c_{x,y+1,z}^\dagger c_{x,y,z} + \text{h.c.}) \\
 & + t_z (c_{x,y,z+1}^\dagger c_{x,y,z} + \text{h.c.}) \\
 & + t_{xyz} (c_{x+1,y+1,z+1}^\dagger c_{x,y,z} + \text{h.c.}), \quad (\text{B1})
 \end{aligned}$$

where  $t_{x,y,z}$  are the nearest neighbor hopping strengths along  $x, y$ , and  $z$  directions, respectively. The term  $t_{xyz}$  represents hopping along the cube diagonal direction. The Hamiltonian is reciprocal and non-Hermitian when the hopping strengths are complex values. Without loss of generality, we choose the  $xy$ -planar basis, and write down the Hamiltonian within this basis

$$H = \sum_z \sum_{l=0,\pm 1} \mathbf{c}_z^\dagger \mathbf{h}_l \mathbf{c}_{z+l}, \quad (\text{B2})$$

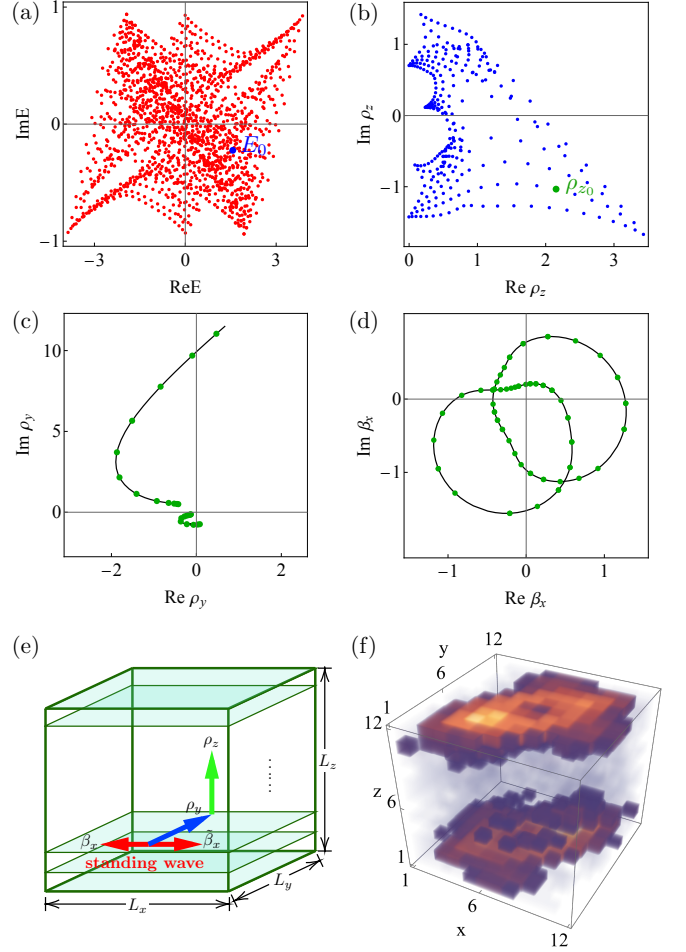


FIG. 5. Numerical verification of the 3D GBZ formula is presented using the tight-binding model Hamiltonian in Eq. (B1) [or Eq. (48)]. (a) shows the OBC eigenvalues as red dots, with the selected eigenvalue  $E_0$  marked by a green dot. (b)-(d) illustrate the GFS for the OBC eigenvalue  $E_0$ . (b) shows the transfer matrix eigenvalues  $\rho_z$ , with the selected value  $\rho_{z_0}$  indicated by a green dot. For  $\rho_{z_0}$ , the 3D Hamiltonian simplifies to a 2D subsystem, and the sub GFS for this subsystem is determined; its projections onto  $\rho_y$  and  $\beta_x$  planes are illustrated in (c) and (d), respectively. (e) visualizes the formation of a standing wave component for the 3D OBC eigen wavefunction. The standing wave is formed along the  $x$  direction by two equal-amplitude non-Bloch waves, where  $|\beta_x| = |\tilde{\beta}_x|$ . (f) shows the constructed 3D wavefunction of energy  $E_0$  using the GFS basis, which fully agrees with the numerical wavefunction obtained by diagonalizing the Hamiltonian matrix. The system parameters specified in Eq. (B1) are  $t_x = t_y = 1/2$ ,  $t_z = 1$ ,  $t_{xyz} = i/2$ , and the system size is  $L_x = L_y = L_z = 12$ .

where  $\mathbf{c}_z^\dagger$  represents a planar creation operator that encompasses all creation operators at the  $z$  plane, specifically  $\mathbf{c}_z^\dagger = \{c_{1,1,z}^\dagger, \dots, c_{L_x,1,z}^\dagger, \dots, c_{1,L_y,z}^\dagger, \dots, c_{L_x,L_y,z}^\dagger\}$ . Here, the lattice size is taken to  $L_x \times L_y \times L_z$ . Therefore, the length of vector  $\mathbf{c}_z^\dagger$  is  $L_x \times L_y$ , and under this basis  $\mathbf{h}_l$  represents a matrix of dimension  $L_x \times L_y$ . The subscript  $l$  denotes the hopping range along the  $z$  direction. The bulk eigenequation can

be transformed into a recursion equation along the  $z$  direction

$$\mathbf{h}_{-1} \psi_{z-1} + (\mathbf{h}_0 - E \mathbb{I}_{L_x \times L_y}) \psi_z + \mathbf{h}_1 \psi_{z+1} = 0. \quad (\text{B3})$$

Here, the planar component  $\psi_z$  can be represented as  $\psi_z = (\Psi_{1,1,z}, \dots, \Psi_{L_x,1,z}, \dots, \Psi_{1,L_y,z}, \dots, \Psi_{L_x,L_y,z})^T$ , with  $\Psi_{x,y,z}$  denoting the wavefunction component at lattice  $(x, y, z)$ . Finally, the transfer matrix can be obtained by writing the recursion equation into a matrix form

$$\begin{pmatrix} \psi_{z+1} \\ \psi_z \end{pmatrix} = \mathbb{T}(E) \begin{pmatrix} \psi_z \\ \psi_{z-1} \end{pmatrix} \quad (\text{B4})$$

$$= \begin{pmatrix} \mathbf{h}_1^{-1} (E \mathbb{I}_{L_x \times L_y} - \mathbf{h}_0) & -\mathbf{h}_1^{-1} \mathbf{h}_{-1} \\ \mathbb{I}_{L_x \times L_y} & 0 \end{pmatrix} \begin{pmatrix} \psi_z \\ \psi_{z-1} \end{pmatrix}.$$

The transfer matrix  $\mathbb{T}(E)$  has the dimension of  $2L_x \times L_y$ .

We set the Hamiltonian parameters to  $t_x = t_y = 1/2$ ,  $t_z = 1$ ,  $t_{xyz} = i/2$ , and take the system size as  $L_x = L_y = L_z = L = 12$ . The corresponding OBC eigenvalues are plotted by the red dots in Fig. 5(a). We pick up a generic OBC eigenvalue  $E_0 = 1.55391 - 0.22258i$  (the blue dot) and calculate its GFS. According to our formula discussed in Sec. V, the bulk allowable  $\rho_z$  values can be solved as the eigenvalues of the transfer matrix  $\mathbb{T}(E_0)$ . These  $2L^2$  values of  $\rho_z$  are plotted by the blue dots in Fig. 5(b), which spans a finite area in the complex  $\rho_z$  plane. Hence, we have  $\dim \rho_z = 2$ . For each fixed  $\rho_z$ , the 3D Hamiltonian reduces to a 2D subsystem, which can be solved using the layer transfer matrix approach once again. Here, we show the results that for a fixed  $\rho_{z_0} = 2.15655 - 1.03812i$ , the sub GFS for the 2D subsystem is solved and its projections onto  $\rho_y$  and  $\beta_x$  planes are illustrated in Figs. 5(c) and (d), respectively. Here, for the 2D subsystem, layer- $y$  basis has been selected. For each fixed  $\rho_z$ ,

the GFS for the corresponding 2D subsystem forms 1D curves in  $(\beta_x, \rho_y)$  space. Meanwhile,  $\rho_z$  spans a finite region. Consequently, GFS corresponding to a specific energy  $E_0$  manifests as a 3D manifold. As  $E_0$  sweeps through the entire OBC continuum spectrum, the collection of GFSs constitutes the GBZ, which is a 5D manifold. Therefore, through Figs. 5(a)-(d), we numerically verified the dimensions for GFS and GBZ using the 3D tight-binding model in Eq. (B1).

Now we examine the OBC wavefunctions using the GFS/GBZ basis. According to Eq. (13), the number of standing wave conditions is  $2d - \dim \text{GBZ} = 1$ . It means that one can enforce the standing wave condition along either one direction. Based on the basis we choose above, the standing waves are formed in the  $x$  direction. An illustration of a standing wave component of an OBC eigen wavefunction is shown in Figs. 5(e). The standing wave is first formed along the  $x$  direction, and then transfer along the  $y$  and  $z$  directions. Therefore, the OBC wavefunction can be constructed as follows

$$\Psi_{E_0}(x, y, z) = \sum_{i=1}^{2L^2} \sum_{j=1}^{2L} A_{ij} \rho_{z,i}^z \rho_{y,j}^y (\beta_{x,1}^x - \beta_{x,2}^x), \quad (\text{B5})$$

where  $\rho_z$ ,  $\rho_y$ , and  $\beta_x$  are taken on the 3D GFS of energy  $E_0$ . The superposition coefficients  $A_{ij}$  can be determined by applying the open boundary conditions (or termed zero boundary conditions). We obtain the coefficients  $A_{ij}$  by solving the boundary matrix, and plot the constructed wavefunction of Eq. (B5) in Figs. 5(f), which fully coincides with the numerical wavefunction by diagonalizing the Hamiltonian matrix. This agreement in OBC wavefunction validates the 3D GBZ formula presented in Sec. V.

- 
- [1] Yuto Ashida, Zongping Gong, and Masahito Ueda, “Non-Hermitian physics,” *Advances in Physics* **69**, 249–435 (2020).
- [2] Emil J. Bergholtz, Jan Carl Budich, and Flore K. Kunst, “Exceptional topology of non-hermitian systems,” *Rev. Mod. Phys.* **93**, 015005 (2021).
- [3] Kun Ding, Chen Fang, and Guancong Ma, “Non-hermitian topology and exceptional-point geometries,” *Nature Reviews Physics* **4**, 745–760 (2022).
- [4] Bo Zhen, Chia Wei Hsu, Yuichi Igarashi, Ling Lu, Ido Kaminer, Adi Pick, Song-Liang Chua, John D. Joannopoulos, and Marin Soljačić, “Spawning rings of exceptional points out of Dirac cones,” *Nature* **525**, 354–358 (2015).
- [5] Hengyun Zhou, Chao Peng, Yoseob Yoon, Chia Wei Hsu, Keith A. Nelson, Liang Fu, John D. Joannopoulos, Marin Soljačić, and Bo Zhen, “Observation of bulk Fermi arc and polarization half charge from paired exceptional points,” *Science* **359**, 1009–1012 (2018).
- [6] Alexander Cerjan, Sheng Huang, Mohan Wang, Kevin P. Chen, Yidong Chong, and Mikael C. Rechtsman, “Experimental realization of a weyl exceptional ring,” *Nature Photonics* **13**, 623–628 (2019).
- [7] Lujun Huang, Sibao Huang, Chen Shen, Simon Yves, Artem S. Pilipchuk, Xiang Ni, Seunghwi Kim, Yan Kei Chiang, David A. Powell, Jie Zhu, Ya Cheng, Yong Li, Almas F. Sadreev, Andrea Alù, and Andrey E. Miroshnichenko, “Acoustic resonances in non-hermitian open systems,” *Nature Reviews Physics* **6**, 11–27 (2024).
- [8] Li Zhang, Yihao Yang, Yong Ge, Yi-Jun Guan, Qiaolu Chen, Qinghui Yan, Fujia Chen, Rui Xi, Yuanzhen Li, Ding Jia, Shou-Qi Yuan, Hong-Xiang Sun, Hongsheng Chen, and Baile Zhang, “Acoustic non-hermitian skin effect from twisted winding topology,” *Nature Communications* **12**, 6297 (2021).
- [9] Colin Scheibner, Anton Souslov, Debarghya Banerjee, Piotr Surówka, William T. M. Irvine, and Vincenzo Vitelli, “Odd elasticity,” *Nature Physics* **16**, 475–480 (2020).
- [10] Colin Scheibner, William T. M. Irvine, and Vincenzo Vitelli, “Non-Hermitian Band Topology and Skin Modes in Active Elastic Media,” *Phys. Rev. Lett.* **125**, 118001 (2020).
- [11] Di Zhou and Junyi Zhang, “Non-hermitian topological metamaterials with odd elasticity,” *Phys. Rev. Res.* **2**, 023173 (2020).
- [12] Debarghya Banerjee, Vincenzo Vitelli, Frank Jülicher, and Piotr Surówka, “Active viscoelasticity of odd materials,” *Phys. Rev. Lett.* **126**, 138001 (2021).
- [13] Suraj Shankar, Anton Souslov, Mark J. Bowick, M. Cristina Marchetti, and Vincenzo Vitelli, “Topological active matter,” *Nature Reviews Physics* **4**, 380–398 (2022).



- [14] Fei Song, Shunyu Yao, and Zhong Wang, “Non-hermitian skin effect and chiral damping in open quantum systems,” *Phys. Rev. Lett.* **123**, 170401 (2019).
- [15] Chun-Hui Liu, Kai Zhang, Zhesen Yang, and Shu Chen, “Helical damping and dynamical critical skin effect in open quantum systems,” *Phys. Rev. Res.* **2**, 043167 (2020).
- [16] Taiki Haga, Masaya Nakagawa, Ryusuke Hamazaki, and Masahito Ueda, “Liouvillian skin effect: Slowing down of relaxation processes without gap closing,” *Phys. Rev. Lett.* **127**, 070402 (2021).
- [17] Wen-Tan Xue, Yu-Min Hu, Fei Song, and Zhong Wang, “Non-hermitian edge burst,” *Phys. Rev. Lett.* **128**, 120401 (2022).
- [18] Dorje C Brody, “Biorthogonal quantum mechanics,” *Journal of Physics A: Mathematical and Theoretical* **47**, 035305 (2013).
- [19] Naomichi Hatano and David R. Nelson, “Localization transitions in non-hermitian quantum mechanics,” *Phys. Rev. Lett.* **77**, 570–573 (1996).
- [20] Kenta Esaki, Masatoshi Sato, Kazuki Hasebe, and Mahito Kohmoto, “Edge states and topological phases in non-Hermitian systems,” *Phys. Rev. B* **84**, 205128 (2011).
- [21] Huitao Shen, Bo Zhen, and Liang Fu, “Topological Band Theory for Non-Hermitian Hamiltonians,” *Phys. Rev. Lett.* **120**, 146402 (2018).
- [22] Zongping Gong, Yuto Ashida, Kohei Kawabata, Kazuaki Takasan, Sho Higashikawa, and Masahito Ueda, “Topological Phases of Non-Hermitian Systems,” *Phys. Rev. X* **8**, 031079 (2018).
- [23] Yuki Nagai, Yang Qi, Hiroki Isobe, Vladyslav Kozii, and Liang Fu, “DMFT Reveals the Non-Hermitian Topology and Fermi Arcs in Heavy-Fermion Systems,” *Phys. Rev. Lett.* **125**, 227204 (2020).
- [24] Shunyu Yao and Zhong Wang, “Edge States and Topological Invariants of Non-Hermitian Systems,” *Phys. Rev. Lett.* **121**, 086803 (2018).
- [25] Flore K. Kunst, Elisabet Edvardsson, Jan Carl Budich, and Emil J. Bergholtz, “Biorthogonal Bulk-Boundary Correspondence in Non-Hermitian Systems,” *Phys. Rev. Lett.* **121**, 026808 (2018).
- [26] Kazuki Yokomizo and Shuichi Murakami, “Non-Bloch Band Theory of Non-Hermitian Systems,” *Phys. Rev. Lett.* **123**, 066404 (2019).
- [27] Ching Hua Lee and Ronny Thomale, “Anatomy of skin modes and topology in non-Hermitian systems,” *Phys. Rev. B* **99**, 201103(R) (2019).
- [28] Dan S. Borgnia, Alex Jura Kruchkov, and Robert-Jan Slager, “Non-hermitian boundary modes and topology,” *Phys. Rev. Lett.* **124**, 056802 (2020).
- [29] Kai Zhang, Zhesen Yang, and Chen Fang, “Correspondence between Winding Numbers and Skin Modes in Non-Hermitian Systems,” *Phys. Rev. Lett.* **125**, 126402 (2020).
- [30] Nobuyuki Okuma, Kohei Kawabata, Ken Shiozaki, and Masatoshi Sato, “Topological Origin of Non-Hermitian Skin Effects,” *Phys. Rev. Lett.* **124**, 086801 (2020).
- [31] Zhesen Yang, Kai Zhang, Chen Fang, and Jiangping Hu, “Non-Hermitian Bulk-Boundary Correspondence and Auxiliary Generalized Brillouin Zone Theory,” *Phys. Rev. Lett.* **125**, 226402 (2020).
- [32] Kohei Kawabata, Nobuyuki Okuma, and Masatoshi Sato, “Non-bloch band theory of non-hermitian hamiltonians in the symplectic class,” *Phys. Rev. B* **101**, 195147 (2020).
- [33] Stefano Longhi, “Probing non-hermitian skin effect and non-bloch phase transitions,” *Phys. Rev. Research* **1**, 023013 (2019).
- [34] Tian-Shu Deng and Wei Yi, “Non-bloch topological invariants in a non-hermitian domain wall system,” *Phys. Rev. B* **100**, 035102 (2019).
- [35] Lei Xiao, Tianshu Deng, Kunkun Wang, Gaoyan Zhu, Zhong Wang, Wei Yi, and Peng Xue, “Non-Hermitian bulk–boundary correspondence in quantum dynamics,” *Nature Physics* **16**, 761–766 (2020).
- [36] T. Helbig, T. Hofmann, S. Imhof, M. Abdelghany, T. Kiessling, L. W. Molenkamp, C. H. Lee, A. Szameit, M. Greiter, and R. Thomale, “Generalized bulk–boundary correspondence in non-Hermitian topoelectrical circuits,” *Nature Physics* **16**, 747–750 (2020).
- [37] Ananya Ghatak, Martin Brandenbourger, Jasper van Wezel, and Corentin Coulais, “Observation of non-Hermitian topology and its bulk–edge correspondence in an active mechanical metamaterial,” *Proceedings of the National Academy of Sciences* **117**, 29561–29568 (2020).
- [38] Linhu Li, Ching Hua Lee, Sen Mu, and Jiangbin Gong, “Critical non-Hermitian skin effect,” *Nature Communications* **11**, 5491 (2020).
- [39] Jahan Claes and Taylor L. Hughes, “Skin effect and winding number in disordered non-hermitian systems,” *Phys. Rev. B* **103**, L140201 (2021).
- [40] Ming Lu, Xiao-Xiao Zhang, and Marcel Franz, “Magnetic suppression of non-hermitian skin effects,” *Phys. Rev. Lett.* **127**, 256402 (2021).
- [41] Chang-An Li, Björn Trauzettel, Titus Neupert, and Song-Bo Zhang, “Enhancement of second-order non-hermitian skin effect by magnetic fields,” *Phys. Rev. Lett.* **131**, 116601 (2023).
- [42] Zhongming Gu, He Gao, Haoran Xue, Jensen Li, Zhongqing Su, and Jie Zhu, “Transient non-hermitian skin effect,” *Nature Communications* **13**, 7668 (2022).
- [43] Nan Cheng, Chang Shu, Kai Zhang, Xiaoming Mao, and Kai Sun, “Universal spectral moment theorem and its applications in non-hermitian systems,” (2024), [arXiv:2403.01583](https://arxiv.org/abs/2403.01583).
- [44] Kyrlo Ochkan, Raghav Chaturvedi, Viktor Könye, Louis Veyrat, Romain Giraud, Dominique Mailly, Antonella Cavanna, Ulf Gennser, Ewelina M. Hankiewicz, Bernd Büchner, Jeroen van den Brink, Joseph Dufouleur, and Ion Cosma Fulga, “Non-hermitian topology in a multi-terminal quantum hall device,” *Nature Physics* (2024), [10.1038/s41567-023-02337-4](https://doi.org/10.1038/s41567-023-02337-4).
- [45] Nobuyuki Okuma and Masatoshi Sato, “Non-hermitian topological phenomena: A review,” *Annual Review of Condensed Matter Physics* **14**, 83–107 (2023).
- [46] Rijia Lin, Tommy Tai, Linhu Li, and Ching Hua Lee, “Topological non-hermitian skin effect,” *Frontiers of Physics* **18**, 53605 (2023).
- [47] Xiujuan Zhang, Tian Zhang, Ming-Hui Lu, and Yan-Feng Chen, “A review on non-hermitian skin effect,” *Advances in Physics: X* **7**, 2109431 (2022).
- [48] Tony E. Lee, “Anomalous edge state in a non-hermitian lattice,” *Phys. Rev. Lett.* **116**, 133903 (2016).
- [49] V. M. Martinez Alvarez, J. E. Barrios Vargas, and L. E. F. Foa Torres, “Non-Hermitian robust edge states in one dimension: Anomalous localization and eigenspace condensation at exceptional points,” *Phys. Rev. B* **97**, 121401(R) (2018).
- [50] Ye Xiong, “Why does bulk boundary correspondence fail in some non-hermitian topological models,” *Journal of Physics Communications* **2**, 035043 (2018).
- [51] Ching-Kai Chiu, Jeffrey C. Y. Teo, Andreas P. Schnyder, and Shinsei Ryu, “Classification of topological quantum matter with symmetries,” *Rev. Mod. Phys.* **88**, 035005 (2016).
- [52] Kohei Kawabata, Ken Shiozaki, Masahito Ueda, and Masatoshi Sato, “Symmetry and Topology in Non-Hermitian Physics,” *Phys. Rev. X* **9**, 041015 (2019).
- [53] Yifei Yi and Zhesen Yang, “Non-hermitian skin modes induced

- by on-site dissipations and chiral tunneling effect,” *Phys. Rev. Lett.* **125**, 186802 (2020).
- [54] Wen-Tan Xue, Ming-Rui Li, Yu-Min Hu, Fei Song, and Zhong Wang, “Simple formulas of directional amplification from non-bloch band theory,” *Phys. Rev. B* **103**, L241408 (2021).
- [55] Linhu Li, Sen Mu, Ching Hua Lee, and Jiangbin Gong, “Quantized classical response from spectral winding topology,” *Nature Communications* **12**, 5294 (2021).
- [56] Stefano Longhi, Davide Gatti, and Giuseppe Della Valle, “Robust light transport in non-hermitian photonic lattices,” *Scientific Reports* **5**, 13376 (2015).
- [57] A. McDonald, T. Pereg-Barnea, and A. A. Clerk, “Phase-dependent chiral transport and effective non-hermitian dynamics in a bosonic kitaev-majorana chain,” *Phys. Rev. X* **8**, 041031 (2018).
- [58] Jong Yeon Lee, Junyeong Ahn, Hengyun Zhou, and Ashvin Vishwanath, “Topological correspondence between hermitian and non-hermitian systems: Anomalous dynamics,” *Phys. Rev. Lett.* **123**, 206404 (2019).
- [59] Takumi Bessho and Masatoshi Sato, “Nielsen-ninomiya theorem with bulk topology: Duality in floquet and non-hermitian systems,” *Phys. Rev. Lett.* **127**, 196404 (2021).
- [60] Qian Liang, Dizhou Xie, Zhaoli Dong, Haowei Li, Hang Li, Bryce Gadway, Wei Yi, and Bo Yan, “Dynamic Signatures of Non-Hermitian Skin Effect and Topology in Ultracold Atoms,” *Phys. Rev. Lett.* **129**, 070401 (2022).
- [61] Kai Zhang, Chen Fang, and Zhesen Yang, “Dynamical degeneracy splitting and directional invisibility in non-hermitian systems,” *Phys. Rev. Lett.* **131**, 036402 (2023).
- [62] Jan Carl Budich and Emil J. Bergholtz, “Non-hermitian topological sensors,” *Phys. Rev. Lett.* **125**, 180403 (2020).
- [63] Alexander McDonald and Aashish A. Clerk, “Exponentially-enhanced quantum sensing with non-hermitian lattice dynamics,” *Nature Communications* **11**, 5382 (2020).
- [64] Liying Bao, Bo Qi, and Daoyi Dong, “Exponentially enhanced quantum non-hermitian sensing via optimized coherent drive,” *Phys. Rev. Appl.* **17**, 014034 (2022).
- [65] Stefano Longhi, “Self-healing of non-hermitian topological skin modes,” *Phys. Rev. Lett.* **128**, 157601 (2022).
- [66] Zongping Gong, Miguel Bello, Daniel Malz, and Flore K. Kunst, “Anomalous behaviors of quantum emitters in non-hermitian baths,” *Phys. Rev. Lett.* **129**, 223601 (2022).
- [67] Zixi Fang, Chen Fang, and Kai Zhang, “Point-gap bound states in non-hermitian systems,” *Phys. Rev. B* **108**, 165132 (2023).
- [68] Sebastian Weidemann, Mark Kremer, Tobias Helbig, Tobias Hofmann, Alexander Stegmaier, Martin Greiter, Ronny Thomale, and Alexander Szameit, “Topological funneling of light,” *Science* **368**, 311–314 (2020).
- [69] Wei Wang, Xulong Wang, and Guancong Ma, “Non-hermitian morphing of topological modes,” *Nature* **608**, 50–55 (2022).
- [70] Kohei Kawabata, Masatoshi Sato, and Ken Shiozaki, “Higher-order non-Hermitian skin effect,” *Phys. Rev. B* **102**, 205118 (2020).
- [71] Shunyu Yao, Fei Song, and Zhong Wang, “Non-Hermitian Chern Bands,” *Phys. Rev. Lett.* **121**, 136802 (2018).
- [72] Ching Hua Lee, Linhu Li, and Jiangbin Gong, “Hybrid Higher-Order Skin-Topological Modes in Nonreciprocal Systems,” *Phys. Rev. Lett.* **123**, 016805 (2019).
- [73] Tao Liu, Yu-Ran Zhang, Qing Ai, Zongping Gong, Kohei Kawabata, Masahito Ueda, and Franco Nori, “Second-Order Topological Phases in Non-Hermitian Systems,” *Phys. Rev. Lett.* **122**, 076801 (2019).
- [74] Linhu Li, Ching Hua Lee, and Jiangbin Gong, “Topological Switch for Non-Hermitian Skin Effect in Cold-Atom Systems with Loss,” *Phys. Rev. Lett.* **124**, 250402 (2020).
- [75] Deyuan Zou, Tian Chen, Wenjing He, Jiacheng Bao, Ching Hua Lee, Houjun Sun, and Xiangdong Zhang, “Observation of hybrid higher-order skin-topological effect in non-hermitian topoelectrical circuits,” *Nature Communications* **12**, 7201 (2021).
- [76] Xiujian Zhang, Yuan Tian, Jian-Hua Jiang, Ming-Hui Lu, and Yan-Feng Chen, “Observation of higher-order non-hermitian skin effect,” *Nature Communications* **12**, 5377 (2021).
- [77] Kai Zhang, Zhesen Yang, and Chen Fang, “Universal non-hermitian skin effect in two and higher dimensions,” *Nature Communications* **13**, 2496 (2022).
- [78] Yi-Cheng Wang, Jih-Shih You, and H. H. Jen, “A non-hermitian optical atomic mirror,” *Nature Communications* **13**, 4598 (2022).
- [79] Zhening Fang, Mengying Hu, Lei Zhou, and Kun Ding, “Geometry-dependent skin effects in reciprocal photonic crystals,” *Nanophotonics* **11**, 3447–3456 (2022).
- [80] Qiuyan Zhou, Jien Wu, Zhenhang Pu, Jiuyang Lu, Xueqin Huang, Weiyin Deng, Manzhu Ke, and Zhengyou Liu, “Observation of geometry-dependent skin effect in non-hermitian phononic crystals with exceptional points,” *Nature Communications* **14**, 4569 (2023).
- [81] Wei Wang, Mengying Hu, Xulong Wang, Guancong Ma, and Kun Ding, “Experimental realization of geometry-dependent skin effect in a reciprocal two-dimensional lattice,” *Phys. Rev. Lett.* **131**, 207201 (2023).
- [82] Tuo Wan, Kai Zhang, Junkai Li, Zhesen Yang, and Zhaoju Yang, “Observation of the geometry-dependent skin effect and dynamical degeneracy splitting,” *Science Bulletin* **68**, 2330–2335 (2023).
- [83] Yi Qin, Kai Zhang, and Linhu Li, “Geometry-dependent skin effect and anisotropic bloch oscillations in a non-hermitian optical lattice,” *Phys. Rev. A* **109**, 023317 (2024).
- [84] Kai Zhang, Zhesen Yang, and Kai Sun, “Edge theory of non-hermitian skin modes in higher dimensions,” *Phys. Rev. B* **109**, 165127 (2024).
- [85] Zhi-Yuan Wang, Jian-Song Hong, and Xiong-Jun Liu, “Symmetric non-hermitian skin effect with emergent nonlocal correspondence,” *Phys. Rev. B* **108**, L060204 (2023).
- [86] Entong Zhao, Zhiyuan Wang, Chengdong He, Ting Fung Jeffrey Poon, Ka Kwan Pak, Yu-Jun Liu, Peng Ren, Xiong-Jun Liu, and Gyu-Boong Jo, “Two-dimensional non-hermitian skin effect in an ultracold fermi gas,” (2023), [arXiv:2311.07931](https://arxiv.org/abs/2311.07931).
- [87] Kazuki Yokomizo and Shuichi Murakami, “Non-bloch bands in two-dimensional non-hermitian systems,” *Phys. Rev. B* **107**, 195112 (2023).
- [88] Hui Jiang and Ching Hua Lee, “Dimensional transmutation from non-hermiticity,” *Phys. Rev. Lett.* **131**, 076401 (2023).
- [89] Hong-Yi Wang, Fei Song, and Zhong Wang, “Amoeba formulation of non-bloch band theory in arbitrary dimensions,” *Phys. Rev. X* **14**, 021011 (2024).
- [90] Haiping Hu, “Non-hermitian band theory in all dimensions: uniform spectra and skin effect,” (2023), [arXiv:2306.12022](https://arxiv.org/abs/2306.12022).
- [91] Zeqi Xu, Bo Pang, Kai Zhang, and Zhesen Yang, “Two-dimensional asymptotic generalized brillouin zone theory,” (2023), [arXiv:2311.16868](https://arxiv.org/abs/2311.16868).
- [92] Kai Sun, Anton Souslov, Xiaoming Mao, and T. C. Lubensky, “Surface phonons, elastic response, and conformal invariance in twisted kagome lattices,” *Proceedings of the National Academy of Sciences* **109**, 12369–12374 (2012).
- [93] D. H. Lee and J. D. Joannopoulos, “Simple scheme for surface-band calculations. i,” *Phys. Rev. B* **23**, 4988–4996 (1981).
- [94] Yasuhiro Hatsugai, “Edge states in the integer quantum hall ef-

- fect and the riemann surface of the bloch function,” *Phys. Rev. B* **48**, 11851–11862 (1993).
- [95] Vatsal Dwivedi and Victor Chua, “Of bulk and boundaries: Generalized transfer matrices for tight-binding models,” *Phys. Rev. B* **93**, 134304 (2016).
- [96] Flore K. Kunst and Vatsal Dwivedi, “Non-hermitian systems and topology: A transfer-matrix perspective,” *Phys. Rev. B* **99**, 245116 (2019).
- [97] Albrecht Böttcher and Bernd Silbermann, *Introduction to large truncated Toeplitz matrices* (Springer Science & Business Media, 2012).